

POLITECNICO DI TORINO

Master's Degree in Biomedical Engineering



**Politecnico
di Torino**

Master's Degree Thesis

A quantitative study on the effect of applied probe pressure during OCTA skin acquisitions

Supervisors

Prof. Kristen Mariko MEIBURGER

Ing. Giulia ROTUNNO

Ing. Lisa KRAINZ

Prof. Mengyang LIU

Candidate

ANTONELLA MANDRACCHIA

Academic Year 2024/2025

Summary

Optical Coherence Tomography Angiography (OCTA) is an emerging non-invasive, high-resolution imaging technique used in dermatology for visualizing skin vasculature. Images are acquired through a probe brought in contact with the skin surface; however, this modality can introduce mechanical stress to the skin and temporarily change the underlying vascular structure, compromising the accuracy of OCTA images.

Therefore, the pressure applied by the OCTA probe is a critical factor that can affect the repeatability of acquisitions and reliability of the resulting data.

This thesis aims to analyze how OCTA probe pressure may affect the accuracy and quality of angiographic images, evaluating the impact via specific metrics and validating the results through statistical analysis. For this study, 10 acquisitions were taken on healthy volunteers at the Medical University of Vienna, in three different anatomical regions (arm, head, leg), for a total of 53 OCTA volumes. Data was taken by maintaining constant contact between probe and skin surface, but progressively increasing the applied force, in a range from 1 to 10 Newtons. The OCTA probe was equipped with a force sensor for real-time measurement and data collection during acquisition. Using data processing algorithms, OCTA images were reconstructed from the raw OCT volumes through an intensity-based-method, followed by a dedicated artifact attenuation pipeline. At this processing stage, the Mean Noise Level and PSNR (Peak Signal-to-Noise Ratio) were calculated to assess the amount of noise in the volumes. Then, from the OCTA volumes, two 2D projections were derived, one for the superficial layer and one for the deep layer. Additional image quality metrics (BRISQUE, NIQE and PIQE), texture parameters such as entropy and skewness, and vascular features such as vascular density were estimated.

To evaluate the influence of pressure on image quality and to determine an ideal range pressure for each imaging location, statistical analyses, including linear regression and ANOVA test, were performed to assess differences between layers and

anatomical regions. An increase in pressure is observed to have a greater impact on the superficial layer than on the deep layer. As the applied pressure increases, there is a noticeable change in noise-related parameters ($p\text{value} < 0.05$), which appears to influence image characteristics. In contrast, a comparison between different acquisitions reveals a decrease in vascular density (-2.35% arm, -2.28% head, -5.30% leg), suggesting a modification in structural details and highlighting how pressure variations can affect vascular features. Among the body locations analyzed, the head appears to be more sensitive to pressure, distinguished by greater variation in metrics. Ultimately, the optimal pressure range varies according to the anatomical region considered. However, the presence of artifacts in OCTA images due to involuntary movements is a limitation of this study, as is the reduced sample size analyzed. In addition, the analysis of only three body areas does not allow the results to be generalized to other skin regions.

This thesis aims to establish guidelines for controlled pressure in OCTA acquisitions, enhancing image quality and parameter reliability for accurate analysis of superficial skin microvasculature. The results show that pressure noticeably impacts image quality and vascular features, with optimal ranges varying by anatomical region, providing a reference for standardized imaging protocols.

Table of Contents

List of Tables	VII
List of Figures	VIII
1 Introduction	1
1.1 Clinical target: human skin	1
1.2 OCT and OCTA	4
1.2.1 OCT Principles	4
1.2.2 OCTA Principles	7
1.2.3 Force Sensors	10
1.3 Pressure	12
1.3.1 Pressure in human body	12
1.3.2 Pressure in imaging devices	14
1.3.3 Pressure role in skin OCTA acquisition	15
2 Materials and methods	17
2.1 Data acquisition	18
2.2 Image Processing	22
2.2.1 Raw Data Processing	22
2.2.2 OCTA Reconstruction	24
2.2.3 Artifact Removal	27
2.3 Evaluation Metrics	31
2.3.1 Noise parameters: Mean Noise Level and PSNR	32
2.3.2 Image Quality metrics	33
2.3.3 Texture metrics	34
2.3.4 Vascular Density	35
2.3.5 Computation of metrics	36
3 Results	39

4 Discussion	57
4.0.1 Effects of pressure on image quality	57
4.0.2 Analysis by anatomical regions	59
4.0.3 Pressure impact on vascular density	62
4.0.4 Optimal pressure range	64
4.1 Limitations	65
5 Conclusions and Future Developments	66
Bibliography	68

List of Tables

1.1	<i>Physiological pressures in the human body (in mm Hg).</i>	13
3.1	Optimal pressure range for each anatomical region and layer.	56

List of Figures

1.1	<i>Representation of the layers of the skin (left) and the different substrates of the epidermis (right) [4].</i>	3
1.2	<i>Scheme of Michelson interferometer [8].</i>	5
1.3	<i>Representation of OCT system based on Michelson interferometer [9].</i>	6
1.4	<i>Fourier Domain OCT: Shown in the figure are the SD-OCT system (left) and the SS-OCT system (right) [15].</i>	8
1.5	<i>Graphical representation of the OCTA prototype employed for image acquisition.</i>	9
1.6	<i>Image shows a force sensor assembled on a metal structure, with a 3D model (left) and a dimensioned technical drawing (right) [22]. . .</i>	10
1.7	<i>Photo of a pressure sensor with which the probe of the OCT system used is equipped.</i>	11
1.8	<i>Effect of OCTA probe pressure on blood vessels: it is seen that high probe pressure can alter the underlying vascular network distorting the recorded signal [33].</i>	16
2.1	<i>OCT prototype present at MUW, with which acquisitions were made.</i>	19
2.2	<i>Image of the slide interposed in the OCT probe used in the laboratory.</i>	21
2.3	<i>Of the same acquisition, a cross-section obtained with an inadequate ROI is shown in the first image above. In the second image, the cross-section allows to see all the details instead.</i>	23
2.4	<i>B-scan obtained from an acquisition on the arm, at 8 Newtons. . . .</i>	24
2.5	<i>Cross-section obtained from an acquisition on the arm, at 8 Newtons.</i>	24
2.6	<i>Visualization of the linear fitting (blue line on the surface) used to identify the skin surface.</i>	25
2.7	<i>OCT en-face and Intensity-Angio en-face at different depths, belonging to an acquisition on the leg.</i>	26
2.8	<i>Original OCTA image (left) and image after white line correction (right), in an acquisition on the leg at 4 Newtons.</i>	27
2.9	<i>Original OCTA image (left) and image after projection artifact correction (right), in an acquisition on the arm at 4 Newtons. . . .</i>	28

2.10	Representation of the artifact removal pipeline in the 2 layers, superficial (left coloumn) and deep (right coloumn).	30
2.11	3D graph showing the spatial distribution of Mean Noise Level (MNL) in an acquisition on the arm, in the superficial (left) and deep layer (right).	36
2.12	From top to bottom: MIP, binarized image and skeleton of an OCTA volume acquired on the leg at 6 Newtons. The two columns refer to the two analyzed layers, superficial and deep.	38
3.1	Significant metrics visualization for superficial layer.	40
3.2	Significant metrics visualization for deep layer.	40
3.3	Linear regression result for superficial layer.	41
3.4	Linear regression result for deep layer.	42
3.5	Linear regression result for arm superficial layer.	44
3.6	Linear regression result for arm deep layer.	45
3.7	Linear regression result for head superficial layer.	46
3.8	Linear regression result for head deep layer.	47
3.9	Linear regression result for leg superficial layer.	48
3.10	Linear regression result for leg deep layer.	49
3.11	Boxplot of one-way ANOVA test between different body area.	52
3.12	Percentage variation in vascular density obtained by binarized mask, in the 3 anatomic regions analyzed.	54
3.13	Variation in vascular density obtained by binarized mask, in the 3 anatomical regions as a function of pressure.	54
3.14	Percentage variation in vascular density obtained by skeleton, in the 3 anatomic regions analyzed.	55
3.15	Variation in vascular density obtained by skeleton, in the 3 anatomical regions as a function of pressure.	55
4.1	The two graphs show the spatial distribution of Mean Noise Level (MNL): the first line belongs to an acquisition on the head at 1N, surface layer (left) and deep layer (right) respectively, the second line to the same acquisition but at 10N. One can see, qualitatively, a decrease in the value of MNL.	58
4.2	OCTA images referred to an acquisition on the head, at 1N (A), 2N (B), 4N(C). It can be seen that as the force applied by the probe increases, the vascular structure is no longer detected and is almost absent.	60

4.3 *The first row corresponds to an acquisition of the head, the second to the arm, and the third to the leg. Images in the left column (A, C,E) were taken at the minimum pressure (1N for head, 2N for arm and leg), while the images in the right column (B,D,F) were acquired at the maximum pressure (10N). In line with the results, a decrease in vascular density is observed in the head and leg acquisitions, whereas a slight increase is noticeable in the arm acquisition. 63*

Chapter 1

Introduction

Optical Coherence Tomography Angiography (OCTA) is a noninvasive imaging technique that allows high-resolution visualization of microvascular structures. During OCTA image acquisition, several factors can affect image quality and vascular parameters—one of the most relevant is the pressure applied by the probe.

The first part of the chapter is dedicated to a description of the OCT system, explaining the basic principles of Optical Coherence Tomography (OCT) and its OCTA extension, which allows visualization of the vascular network. Next, the force sensors used to apply and monitor pressure during acquisition is presented, ensuring reproducibility of measurements.

The role of pressure in OCTA imaging of skin is later explored, starting with an overview of pressure in the human body and its physiological implications. Next, the influence of pressure in imaging devices and its relevance in OCTA acquisitions is analyzed. Finally, how pressure variations affect image quality is discussed, highlighting the importance of optimizing acquisition protocols for clinical and research applications.

1.1 Clinical target: human skin

The skin is the largest and heaviest organ of the human body, covering its entire external surface and ranging in thickness from 1 to 4 mm. It plays a primary role in terms of protecting the body, acting as a first-level barrier against injury from the external environment and against pathogens. Key functions of the skin include shielding the body from heat, light, trauma, and infections. More specifically, the skin is decisive in regulating body temperature and defending against

ultraviolet (UV) rays, and maintaining overall homeostasis by controlling fluid loss and providing immunological defense. The action performed by the skin also assumes fundamental importance in sensory perception. The superficial part of the skin contains an extensive network of sensory receptors that contribute to the protective function of the skin by sensing physical, biological, and environmental signals, such as information about temperature, sensation (pleasure or pain), and pressure, and generating relevant responses. Finally, it is highly adaptable, with specialized thicknesses and functions in different areas of the body [1].

Human skin is composed of three distinct layers: epidermis, dermis, and hypodermis, with varying degrees of specialization within each layer [2], as highlighted in Fig.2.6

- **Epidermis**

The epidermis is the outermost layer of the skin, providing an impermeable barrier and contributing to the tone of the skin. Its thickness varies between 0.05-1.5mm (depending on the body part: 0.05mm on the eyelids to 1.5mm on the palm of the hands and soles of the feet) and it is avascular; meaning it doesn't have any blood vessels. The epidermis is composed of stratified and keratinized squamous cells [3] and can be further divided into other epithelial sublayers: stratum corneum, stratum lucidum, stratum granulosum, stratum spinosum or prickle cell layer, and stratum germinativum or stratum basale. Each sublayer is mainly composed of a specific cell type that performs a particular function. The epidermis has the main role of protecting the body by creating a barrier against external agents and UV radiation. The keratinocyte cells from which it is composed ensure impermeability, preventing water loss, and maintaining hydration. The basal layer of the epidermis is responsible for continuous cell regeneration, a process that ensures cell turnover and promotes the repair of surface lesions.

- **Dermis**

The dermis is usually <2mm thick but can be up to 4mm, depending on the body part considered. It lies beneath the epidermis and is composed mainly of connective tissue rich in collagen and elastin fibers, which confer strength, elasticity and flexibility to the skin. It is divided into two main layers: the papillary dermis (more superficial layer) characterized by fine fibers and capillaries which connect it to the epidermis, and the reticular dermis (deeper layer) composed of dense collagen fibers that provide elasticity and strength. Due to its composition of collagen and elastin, the dermis is responsible for most of the skin's mechanical strength, it also regulates body temperature

and contributes to sensory perception.

- **Hypodermis**

The hypodermis, also known as the subcutaneous layer, lies beneath the dermis and connects the skin to the underlying fascia of muscles and bones. While not technically part of the skin, the distinction between the hypodermis and dermis is often hard to identify. It is made up of loose connective tissue and fat, which acts as a reservoir for fat storage, provides insulation, and offers cushioning. Blood vessels that supply the skin originate in the hypodermis, with capillaries extending into the dermis and epidermis.

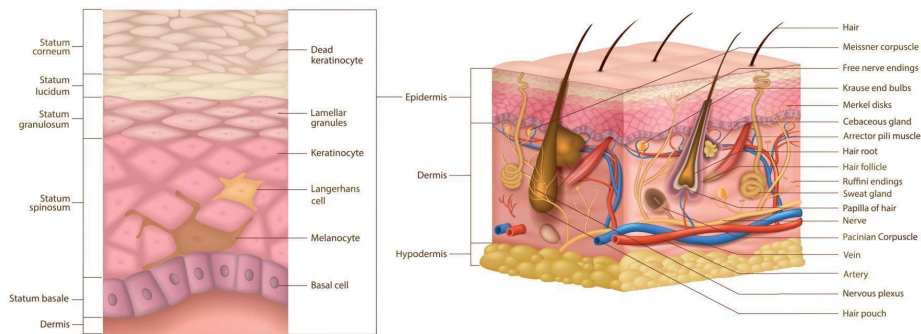


Figure 1.1: Representation of the layers of the skin (left) and the different substrates of the epidermis (right) [4].

The layered structure of the skin, with its varying degrees of thickness, is a major contributor to how it interacts with diagnostic imaging technologies. Noninvasive imaging modalities, in particular, build on the optical and vascular properties of the skin to visualize its microcirculation and structural integrity. However, the mechanical properties of the skin, including its elasticity and response to external forces such as pressure, can significantly affect the quality of the images obtained. Indeed, pressure applied during image acquisition can deform the skin, altering blood flow within the microvasculature and compromising results reliability.

1.2 OCT and OCTA

Optical coherence tomography (OCT) provides a noninvasive imaging methodology characterized by an extremely high resolution in the micrometer range. Developed in the early 1990s to enable *in vivo* analysis of the human eye, it has rapidly gained importance in numerous scientific and clinical fields. Technological developments such as angiography, polarization-sensitive OCT, and elastography have enabled increasingly widespread use of this imaging technique, including in-depth analysis of blood vessels and detection of tumor margins [5]. High-definition observation of internal organs and their pathologies also is made possible by the use of devices such as OCT endoscopes. Finally, in many multimodal imaging techniques, OCT is used as a fundamental tool for the analysis of tissue morphological structure [6].

In this thesis study, the OCT prototype in the Center for Medical Physics and Biomedical Engineering at the Medical University of Vienna (MUW) was used for all the acquisitions.

In the following sections, the characteristics and modes of operation of the OCT system will be analyzed.

1.2.1 OCT Principles

Optical coherence tomography (OCT) is a non-invasive imaging technique that provides detailed three-dimensional images of internal sections of biological specimens. It is positioned between superficial and deep imaging techniques, offering high resolution without requiring tissue excision or treatment.

The functional principle behind OCT imaging is light interference: it is a phenomenon due to the superposition, at one point in space, of two or more waves. Given a light source, if it is divided into 2 paths and then recombined, then interference can be observed [7].

It is then possible to observe that the intensity of the resulting wave at that point can vary between a maximum, which is greater than the sum of the two intensities of the starting waves, and a minimum, at which the waves weaken each other until they annihilate, in which case no wave phenomenon occurs. In reference to this behavior we speak of constructive interference, in the first case, and destructive, in the second.

The term coherence, on the other hand, refers to the ability of light to interfere with itself. The light used in the OCT system is broadband, and because of this characteristic it interferes with itself only when the optical paths coincide exactly. In this case it is said to have low coherence.

In OCT, light reflections are measured by an interferometer, a device capable of realizing this division and recombination of waves, exploiting the low coherence

properties of a broadband light source: only light that has traveled approximately the same distance in the two arms of the interferometer is capable of creating interference bands.

There are various types of interferometer; to describe the operation of the OCT system, reference will be made to the Michelson interferometer, shown in Fig.1.2

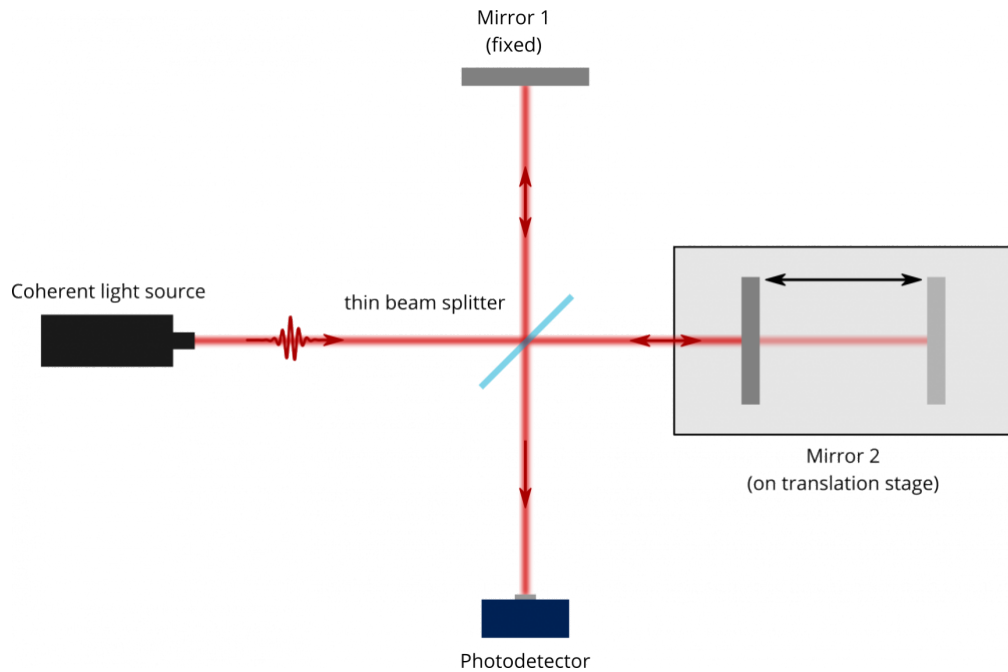


Figure 1.2: *Scheme of Michelson interferometer [8].*

As shown in Fig.1.3, from a low-coherence source, used in an OCT system, near-infrared light is emitted and split into two different paths, toward the two arms of the interferometer: one is considered the reference arm, while the other is the arm destined for the sample to be analyzed.

Light directed toward the reference arm travels until it reaches a reference mirror, which reflects and sends it back, propagating along the same path of origin but in the opposite direction. Conversely, in the sample arm, light is directed toward the sample, where some of it is absorbed or passes through the tissue, while another part is reflected and scattered back due to changes in the refractive index of the different layers of the tissue itself. The return light from both arms recombines at the coupler and generates an interference pattern, which occurs only when the light reflected from the sample travels the same optical distance as the light in the reference arm.

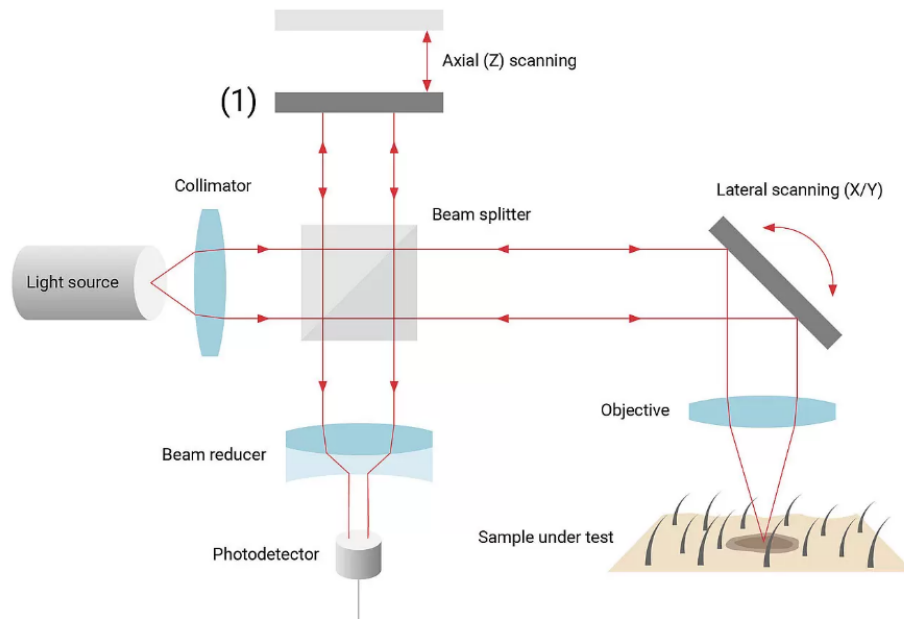


Figure 1.3: Representation of OCT system based on Michelson interferometer [9].

There are 2 different types of OCT, which differ in image acquisition, scan speed, axial and transverse resolution, and imaging field.

Time-domain OCT (TD-OCT) is a first-generation technology that uses a low-coherence light source and a reference scan delay. It actually measures the time delay and the amount of backscattered light from different tissue depths, corresponding to the position of the reference mirror, to obtain two-dimensional images. To probe different depths in the specimen, the distance in the reference arm can be changed: by moving the reference mirror, the path length of the reference light is varied, and in this way, for each position of the mirror, interference occurs only with light that has been reflected from a given depth in the specimen. However, TD-OCT acquires only one point at a time, as it requires mechanical displacement of the reference mirror to obtain information from different depths, and has limited axial resolution. This has enabled the development of new OCT technologies, such as Fourier Domain OCT (FD-OCT).

Detection in Fourier Domain OCT can be done in two ways: either using a spectrometer, called Spectral Domain OCT (SD-OCT) or using a fast-tuning laser, called Swept Source OCT (SS-OCT) (Fig.1.4). Both approaches have in common that reflectivity along a depth profile is measured for a multitude of wavelengths

separately.

SD-OCT uses the same broadband light source as TD-OCT but measures the interferometric light spectrum by a high-resolution spectrometer in the detector arm. The recorded interferogram is then processed with a Fourier Transform to generate the B-scan image. It is characterized by its high acquisition speed and higher resolution in the images.

A tunable laser, that is, a laser whose wavelength can vary over time, on the other hand, is the light source used in the SS-OCT system. In this case, the reference arm has a fixed optical path length but there is a high-speed photodiode in the sample arm. The longer wavelength of the laser source allows deeper penetration into tissue and a higher scanning speed. A single sweep of the laser wavelength produces an A-scan, digitizing the entire spectrum. Next, the digitized signal is processed using the Fourier Transform, allowing reconstruction of the depth profile of light scattered by the sample. SS-OCT systems have been developed to operate at wavelengths between 1050 and 1700 nm; they offer greater imaging depth than SD-OCT because lasers naturally have narrow linewidths, which correspond to the resolution of a spectrometer in SD-OCT [10], [11], [12].

Through mirror displacement, the OCT system records A-scan profiles, a one-dimensional scan that measures the reflectance of light deep within a tissue. To obtain a cross-sectional image, the light beam is shifted laterally across the surface of the tissue and a series of A-scans are acquired sequentially at adjacent locations on the specimen thus obtaining a B-scan, a two-dimensional scan. If multiple 2D images are acquired as neighboring planes, a 3D image, a C-scan, can be constructed [13],[14].

1.2.2 OCTA Principles

Angiography obtained with optical coherence tomography (OCTA) is classified as a non-invasive, high-resolution imaging technique that visualizes the architecture of blood vessels and allows detailed three-dimensional study of blood flow within vascular structures. To date, OCTA represents the most successful functional extension of OCT because it can be integrated on any OCT platform [14], [16].

In OCTA, angiographic images are obtained without the need to administer contrast medium: in fact, this technique takes advantage of motion contrast imaging, i.e., contrast generated by the natural movement of erythrocytes within blood vessels, which, due to their biconcave structure, reflect light.

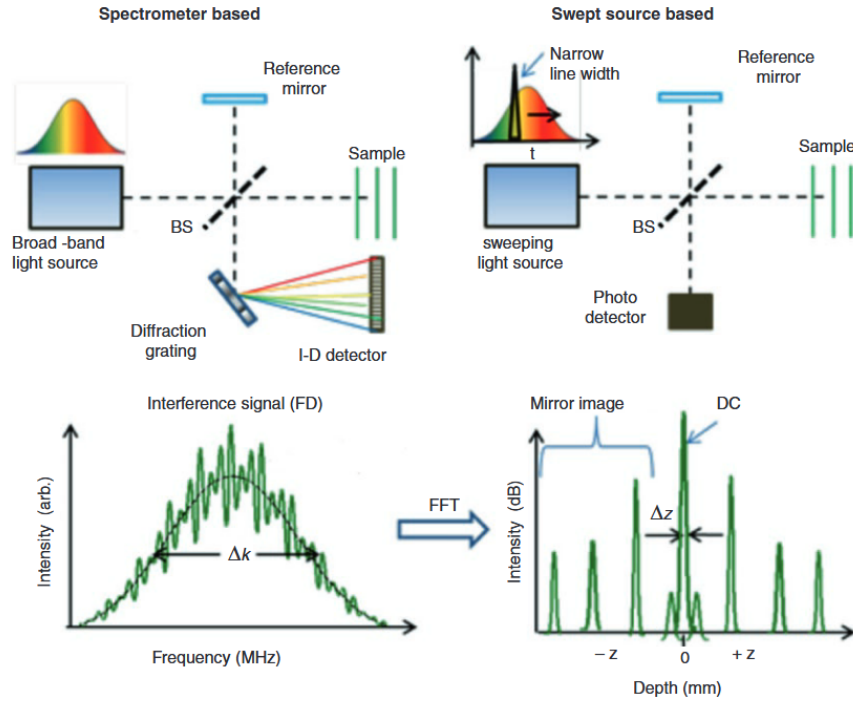


Figure 1.4: *Fourier Domain OCT: Shown in the figure are the SD-OCT system (left) and the SS-OCT system (right) [15].*

The operating principle of OCTA is based on the detection of dynamic structural changes between successive tomograms. In fact, by analyzing consecutive B-scans acquired at the same location, they will be largely similar except for the movement of blood within the tissue; in fact, at locations where blood flow is present, reflectivity and light scattering change from one scan to another. It is therefore possible to visualize blood flow by identifying differences between images on a pixel-by-pixel basis. Specifically, differences in amplitude, intensity, or phase variance between sequential B-scans acquired in the same cross section are calculated, then the decorrelation signal, i.e., differences in the intensity or amplitude of the backscattered OCT signal, is quantified. This method allows only the moving components of the acquisition, i.e., the erythrocytes in the bloodstream, to be visualized. This process is repeated for different locations of the analyzed sample in order to obtain a three-dimensional dataset and map of the blood flow.(Fig.1.5)

Traditional angiographic techniques, such as fluorescein angiography (FA) and

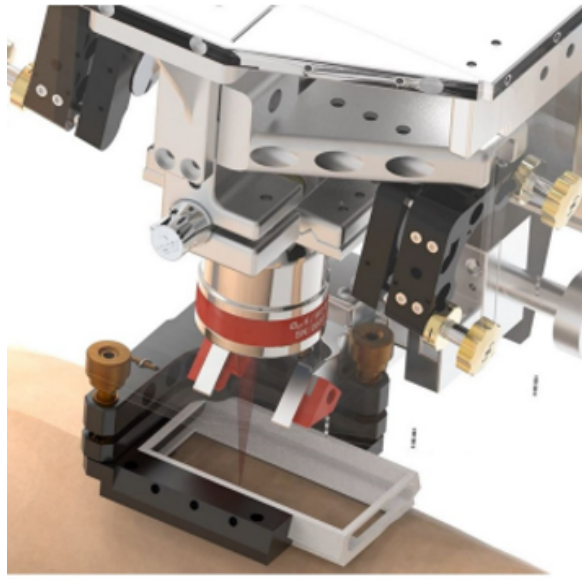


Figure 1.5: *Graphical representation of the OCTA prototype employed for image acquisition.*

indocyanine green angiography (ICGA), are both invasive examinations that involve the introduction of chemical dyes into the vein to visualize flow, and image acquisition is time-consuming. They also provide two-dimensional image sets that allow dynamic visualization of blood flow [17], [18].

In comparison, the OCTA system offers several advantages over the previous two types of angiography. First, the short acquisition time (about 6 seconds) and the absence of a contrast agent allow angiographic analysis to be performed multiple times in a single imaging session to obtain complete information, plus avoiding the risks associated with dye injection. Unlike fluorangiography (FA) or indocyanine green angiography (ICGA), OCTA images are not obscured by hyperfluorescence due to dye leakage, thus allowing for high-contrast, well-defined images of the microvasculature. In addition, structural OCT data are acquired simultaneously with the OCTA data, thus allowing the visualization of en face and cross-sectional images that are perfectly aligned with the angiographic data. This allows depth-layered qualitative and quantitative analysis, facilitating the study of vessel structure in specific areas of the tissue examined.

However, angiography obtained by this imaging technique is not entirely without limitations. It is highly sensitive to motion, and artifacts may manifest as white or black lines or cause misalignment of the vasculature of the specimen being analyzed.

OCTA also cannot assess changes in vascular permeability, which are clearly visible with FA or ICGA. Finally, the appearance of OCTA images is highly dependent on the characteristics of the OCT instrument, scanning protocols, signal processing, and methods used to generate angiographic images from structural OCT data [19], [20], [21].

1.2.3 Force Sensors

To ensure accurate control of the pressure applied during OCTA image acquisition, three force sensors were used and placed on the acquisition probe. These devices allow real-time measurement of the force applied to the tissue, ensuring greater reproducibility of experiments and minimizing the risk of uncontrolled pressure changes. The force sensor used for OCTA image acquisition is the KD34s 10N (Fig.1.6), manufactured by ME-Meßsysteme GmbH [22]. This force transducer was designed specifically for the measurement of small forces (nominal capacity of 10N), making it ideal for applications where high accuracy and sensitivity are required, such as in monitoring applied pressure in biomedical imaging.

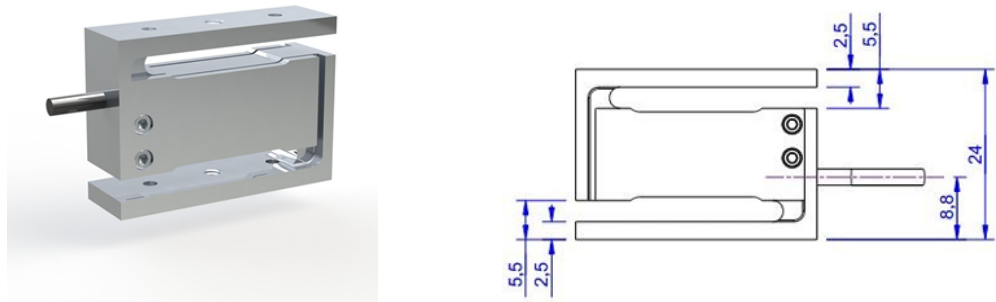


Figure 1.6: Image shows a force sensor assembled on a metal structure, with a 3D model (left) and a dimensioned technical drawing (right) [22].

The KD34s 10N is a strain gauge-based force transducer: the change in electrical resistance of a material when subjected to mechanical deformation is exploited. The sensor consists of a thin conductive grating placed on an elastic surface: when its structure deforms under the action of a force, the change in its length changes the resistance of the grating, converting it into an output signal. This principle ensures high sensitivity and accuracy, and makes the sensor suitable for applications requiring careful control of the pressure applied.

1.3 Pressure

Innumerable physical, biological, and physiological processes are influenced by pressure, a fundamental concept both in the world of research but also in clinical practice. Indeed, it plays a primary role in the general well-being of the human body, especially in the regulation of physiological systems at different levels, but it also affects the accuracy and reliability of modern diagnostic instruments. This section aims to explore the concept of pressure, starting with its physiological significance and analyzing its role in imaging devices, with a focus on skin OCTA imaging.

1.3.1 Pressure in human body

Pressure is a fundamental concept in physics that plays a key role in understanding the behavior of solids, liquids and gases. It is defined as the amount of force exerted per unit area, applied perpendicular to the surface of an object, and it can be determined mathematically using the formula:

$$P = \frac{F}{A}$$

where P denotes the pressure, F denotes the applied force and A represents the area over which the force is distributed.

Pressure is expressed in various units, typically derived by dividing a unit of force by a unit of area. In the International System of Units (SI), pressure is measured in pascals (Pa), where one pascal corresponds to one newton per square meter (N/m^2). More specifically, pressure represents a primary parameter in numerous physical and biological processes. In human physiology, pressure plays a main role in the correct functioning of body systems, such as:

- Cardiovascular system: Systemic arterial pressure, commonly referred to as blood pressure, represents the force that blood exerts on the walls of the large arteries in the flow of the systemic circulation. It depends mainly on cardiac output, the elasticity of the arteries and the resistance in the peripheral vessels. Blood pressure is easily changed by many factors, such as blood volume, resistance of blood vessels, and activity of the autonomic nervous system [23].
- Respiratory system: Breathing is defined as the movement of air in and out of the lungs in an environment with infinite volume and stable external pressure. The physics of normal breathing are based on differential pressure between the lungs and the ambient atmosphere. As the diaphragm and ribcage expand and contract due to muscle action, air flows in and out to balance pressure

[24]. This delicate balance ensures efficient gas exchange and oxygen delivery to tissues.

Although pressure is determinant in the cardiovascular and respiratory systems, it also assumes primary importance in other systems of the human body. For example, in the renal system, pressure influences the filtration of blood through the kidneys, while in the nervous system, balanced pressure is necessary for the homeostasis of the brain and spinal cord. Similarly, in the lymphatic system, pressure contributes to the drainage of interstitial fluids, and in the digestive system, it affects intestinal motility and the process of digestion. For a detailed overview of pressure values in the human body, refer to Tab.1.1.

Body system	Gauge pressure in mm Hg
Blood pressures in large arteries (resting)	
Maximum (systolic)	100–140
Minimum (diastolic)	60–90
Blood pressure in large veins	4–15
Eye	12–24
Brain and spinal fluid (lying down)	5–12
Bladder	
While filling	0–25
When full	100–150
Chest cavity between lungs and ribs	-8 to -4
Inside lungs	-2 to +3
Digestive tract	
Esophagus	-2
Stomach	0–20
Intestines	10–20
Middle ear	<1

Table 1.1: *Physiological pressures in the human body (in mm Hg).*

In the field of diagnostics, pressure measurements represent a critical indicator in the study and the management of numerous pathological conditions. Its simple and non-invasive measurement makes it possible to gather information on the health status of various systems.

For example, to ensure the well-being of the body, it is essential that blood pressure remains within physiological values. In fact, significant alterations, such as low blood pressure levels (hypotension) or high values (hypertension), can cause

serious damage and lead to pathological complications such as induced syncope in the former case, or stroke and myocardial infarction in the latter case.

Also intraocular pressure (IOP), the fluid pressure of the eye, is an essential parameter for the well-being of the eye and for preserving visual capacity over time. IOP exists as a fine-tuned equilibrium between the production and drainage of the aqueous humor, and variations of this delicate balance may have devastating consequences, contributing to the pathogenesis of glaucoma, uveitis, and choroidal detachment [25].

1.3.2 Pressure in imaging devices

Another aspect to consider regarding the use of pressure in clinical settings concerns diagnostic devices, especially imaging equipment. In imaging devices, pressure can directly or indirectly affect the quality and reliability of the obtained images, making its understanding essential for reducing errors and improving diagnostic precision.

Medical imaging can be defined as a set of techniques used to develop visual representations of internal areas of the human body to diagnose potential diseases and consequently monitor their treatment, without the need for surgery or other invasive procedures.

In this context, pressure takes a center stage, as it can affect the accuracy, quality, and reliability of produced images. Different imaging techniques can be sensitive to pressure in various ways, either through direct interaction with the tissues being examined or through the calibration and functionality of the equipment itself. Understanding these dynamics is critical for enhancing diagnostic precision and minimizing errors caused by internal or external factors.

In angiographic techniques, such as computed tomography (TC) and magnetic resonance imaging (MRI), the pressure of the contrast agent injection has a determining part in achieving detailed images of blood vessels. Adequate pressure allows the contrast agent to be injected quickly and to reach the target vessels uniformly: this ensures that the imaging phase coincides with the optimal opacification phase of the vessels. If the injection pressure is too low, the images produced will be poorly detailed or incomplete, as the contrast agent may not reach all areas of interest equally. Conversely, too much pressure could damage the vessels or cause extravasation [26].

In other imaging techniques, however, the pressure exerted by the probe of the instrument used for acquisitions is relevant. For instance, in ultrasound imaging, the pressure applied by the probe in contact with the tissue greatly affects the

quality of the final image. In fact, inadequate pressure could alter temporarily the structure and the shape of soft tissue itself, causing error in the localization of organs and leading to an overall distortion of the image [27, 28].

Similarly, in optical coherence tomography (OCT) and its angiographic variant (OCTA), the pressure applied by the imaging probe on tissues like the retina and skin can cause temporary deformation of these structures, leading to vessels distortions in the captured images. These dynamics pose a challenge for standardization and diagnostic precision, which will be explored in further detail in the chapter *Discussion*.

1.3.3 Pressure role in skin OCTA acquisition

In clinical dermatology, the identification of vascular and structural features of underlying tissues remains a challenge without the use of invasive diagnostic tools. Subcutaneous blood vessels contain relevant information on the health condition or possible disease, such as deep vein thrombosis and peripheral arterial disease. Consequently, visualizing these vessels can help diagnose and monitor various vascular anomaly. For this purpose, accurate visualization systems and image processing algorithms are essential [29, 30].

The most well-known and established imaging techniques, such as MRI, computed tomography angiography and ultrasound, have been reported to visualize skin vasculature, but they have limited resolution that is not high enough to reveal the microvasculature in the superficial layer of skin [31].

Optical coherence tomography (OCT) is an optical tomographic imaging technique that allows non-invasive visualization and measurement of the superficial skin layers. OCT can acquire skin images down to a depth of few millimeters with a high resolution. An extension function based on OCT, OCT angiography (OCTA), provide a image of the skin microvasculature using red blood cell flow as a contrast agent. By acquiring three-dimensional images of the microvasculature, OCTA provides valuable information that enables the evaluation of various subcutaneous features. In addition, the depth and region of the vessels to be analyzed can be precisely selected, thus offering greater repeatability of measurements.

Given their noninvasive and high-resolution characteristics, OCT and OCTA have been increasingly applied in dermatologic research as powerful diagnostic tools. However, image acquisition is performed with the OCT probe in contact with the skin surface: this contact imaging mode can introduce mechanical stress applied to the skin, complicating and sometimes inevitably altering the interpretation of OCT/OCTA imaging results [32]. As shown in Fig. 1.8, excessive probe pressure

compresses the underlying blood vessels, temporarily reducing or preventing blood flow, and compromising proper visualization. This affects the accuracy of OCTA analysis results, and thus its diagnostic ability. It therefore turns out to be a key factor to be able to assess the local pressure applied to the skin during image acquisition, and to understand how this affects the final image.

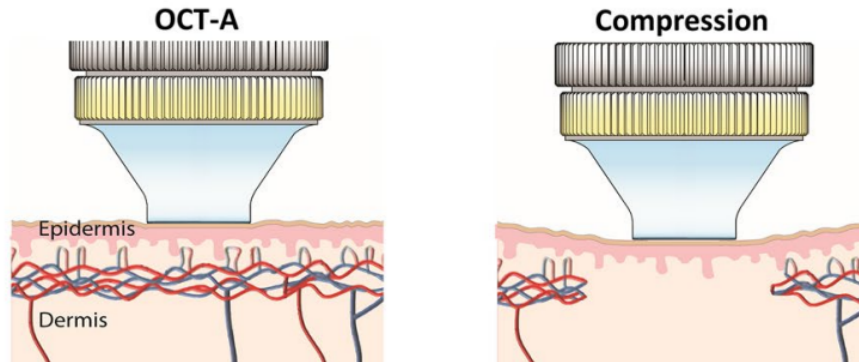


Figure 1.8: *Effect of OCTA probe pressure on blood vessels: it is seen that high probe pressure can alter the underlying vascular network distorting the recorded signal [33].*

In conclusion, this thesis aims to investigate the effects of probe pressure during OCTA skin imaging, focusing on how various pressure levels affect vascular parameters and the overall quality of acquired images. By addressing this critical aspect, the study seeks to improve the diagnostic accuracy and reproducibility of OCTA in clinical dermatology. Subsequent chapters will explain the methodology used to evaluate these effects, present experimental results, and discuss the potential implications for improving OCTA-based diagnostic tools in dermatology practice.

Chapter 2

Materials and methods

This chapter describes the materials and methodologies used for the acquisition, processing, and analysis of images obtained by Optical Coherence Tomography Angiography (OCTA), with particular focus on the instruments used and data processing techniques. The aim is to provide a detailed overview of the procedures adopted to guarantee accurate measurement and evaluation on the quality of OCTA images under controlled pressures.

An explanation of the data acquisition process follows, including the selection of anatomical areas of interest and the experimental conditions adopted to obtain reliable images. Once acquired, the images are processed through a processing pipeline described in the Image Processing section. Finally, evaluation metrics are introduced, which are essential for analyzing image quality and the impact of applied pressure on the parameters of interest.

The experimental approach described in this chapter allows analysis of the effect of pressure on OCTA image quality and vascular density, providing guidelines for interpretation and analysis of the results.

2.1 Data acquisition

This study analyzes data acquired on 7 healthy patients, aged 25-35 years, with a total of 53 OCTA volumes analyzed. The 3 body regions examined were arms, forehead and leg, taking care that for the same area examined the data belonged to different subjects. A total of 10 acquisitions were performed:

- 3 acquisitions in the anatomical region of the arm
- 3 acquisitions in the anatomical region of the forehead
- 4 acquisitions in the anatomical region of the leg

To assess how effectively the force applied by the OCTA system probe affected the quality of the images obtained, all acquisitions were taken by maintaining constant contact between the probe and the skin surface and increasing the force exerted by the probe in a range between 1 and 10 Newtons. Thus, both OCTA and force data are available for each acquisition. All data were collected with the prototype OCT device present in the laboratories of the Center for Medical Physics and Biomedical Engineering at the Medical University of Vienna.

The light source is a swept source laser (SS-OCT-1310, Insight Photonic Solutions, Inc, U.S.), with a scanning frequency of 222.2 kHz (Fig.2.1). In addition, KD34s 10N is the strain gauge force sensor with which the OCT probe is equipped.

As described earlier in Section 2.1.1, in general, the SS-OCT system acquires A-scans, that is, one-dimensional scanning along the z-axis, where each A-scan is generated by a sweeping cycle of the swept source laser. A series of A-scans acquired along the x-direction forms a two-dimensional B-scan. In the acquisitions analyzed in this thesis, 512 A-scans acquired at the same point form a B-scan, and each OCT volume is composed of 512 B-scans acquired consecutively. In addition, 4 OCT volumes acquired at the same location constitute one OCTA volume. At the same time, force data applied by the OCTA prototype probe are also acquired, which is manually adjusted by the operator performing the acquisition. In this study, the force ranges analyzed varied in the range of 2 to 10 Newtons, with the exception of the forehead area where OCTA volumes were also taken at a force value of 1 Newton, for reasons that will be discussed later.



Figure 2.1: *OCT prototype present at MUW, with which acquisitions were made.*

For each acquisition, the protocol described below is followed, consisting of a series of procedures and cautions that ensure the safety of both the study subject and the operator, and also allows for repeatability and accuracy of results.

The steps of the acquisition protocol are as follows:

1. Initial preparation

Before starting the acquisition procedure, the volunteer is placed in a situation of total safety with respect to both the use of the laser by the OCT system and the environment in which he or she is located. In fact, he is made to lie down on a sterile couch in a position of comfort and the area under analysis is uncovered. Also, the volunteer is also asked to wear goggles for the entire duration of the acquisition. This precaution is essential to prevent any risks to which the subject may be exposed due to proximity to the eye area of the laser source, classified as Class 3B. All contact devices used for data acquisition, such as the couch and safety glasses, must be disinfected and sanitized before each imaging session. In addition, the OCT imaging window must also be sterilized after each use.

2. Calibration

System calibration is an essential step to ensure accuracy and reproducibility of the acquired data. When the system is first started, a laser calibration is performed to identify valid OCT image pixels to be considered and those to be excluded because they contain distortion or noise. These datapoints, at the end of the calibration process, are saved in a text file (DVV), which is crucial later for processing the acquired images, as it serves as a guideline on which pixels to consider during subsequent analysis. This procedure is to be performed before each acquisition session to ensure the reliability of the acquired data.

3. Acquisition optimization

In order for image acquisition to produce optimal results, some preliminary steps are performed. The participant is positioned so that the area of interest is exposed in close proximity to the OCT system probe. A 1-mm-thick slide (Fig.2.2) is used between the skin surface and the probe lens to best press the area of interest and avoid the phenomenon of hyper-reflection. In addition, through a pump with a nozzle, a small, evenly distributed amount of distilled water is applied between the skin and the probe glass, to allow a better refractive index matching between those two. Finally, the correct alignment of the laser with the area of interest is verified through an infrared card.

4. Image acquisition

The protocol ends with the actual image acquisition phase. Once the laser has been calibrated and the probe has been properly placed in contact with the skin, a B-scan preview is shown on the display. This step is performed to check image quality and ensure proper contact between the slide and the skin surface. To optimize the visualization of image details, the contact between the probe and the surface analyzed can be improved by adjusting the focus through the device itself and the display scale through the acquisition system. Any changes made can be viewed directly in the B-scan preview. To avoid reflection from the skin surface, the laser beam is tilted with respect to the vertical axis of the skin surface. At this stage, the pressure sensors in the probe are also calibrated; at the moment a suitable B-scan is reached, an applied force of 0 Newton is matched. In order to analyze the influence of probe

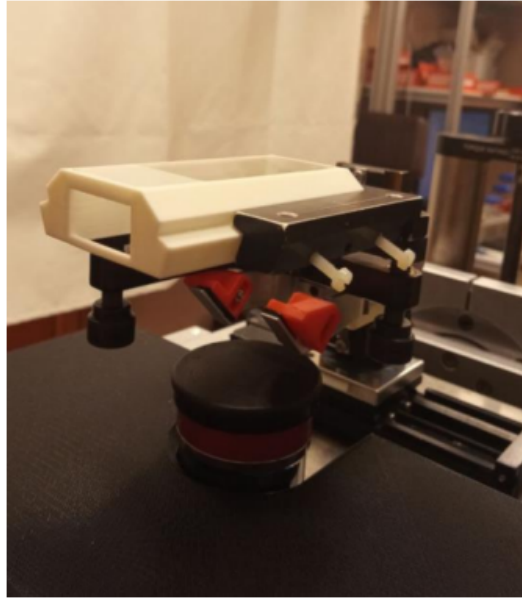


Figure 2.2: *Image of the slide interposed in the OCT probe used in the laboratory.*

pressure on the surface, the area investigated by the probe is kept constant, only the pressure is increased manually by the operator adjusting it through a knob in the probe and checking its intensity on the display. Finally, the image is then acquired (about 20 seconds) and the data of the applied force are saved.

2.2 Image Processing

This section will describe and analyze the processing pipeline used in this study, starting from image acquisition to the extraction of the metrics involved.

2.2.1 Raw Data Processing

The acquired data, organized as raw OCT matrices, are analyzed in the first part of the image processing pipeline, in particular parameters are implemented that will determine the structure and size of the subsequent images.

Values for the size in millimeters of the component voxels of the matrices are then set, in addition, the parameters that define the structure of the acquired data are set, in particular the number of samples per axial scan (the length of the A-scan), the number of A-scans in a B-scan (the transverse resolution of the scan), the number of B-scans per volume (the depth of the scan), and finally the number of B-scans saved in a single file.

It is important to emphasize that at this stage, the most important parameter to define is the Region Of Interest (ROI): it represents a selection of more informative data, reducing computational complexity and processing time. It is pointed out that, in the case of acquisitions made with an increase in the force applied by the probe, it is essential to monitor the B-scan and adjust the ROI accordingly. Keeping an unchanged ROI at high pressures could in fact compromise image quality, reducing the visibility of details and increasing the risk of loss of relevant information. This aspect is particularly recognizable in the display of cross-sections, two-dimensional images on the yz plane, as shown in Fig.2.3.

In the data analyzed in this study, an OCTA volume is composed of a multiple acquisition of 4 OCT volumes at the same location. Each OCT volume consists of 512 B-scans, so there are 2048 B-scans for each acquisition. In order to handle such a large amount of data, the data acquired by the OCT system are organized into 32 files, each containing 64 B-scans. Each of these files is processed individually in order to obtain the final OCTA volume. Finally, for the code to work properly, the DVV file, obtained during the calibration process, is also required.

After loading, once they have been divided into 32 smaller files to optimize their handling, the acquired data are analyzed individually.

A background subtraction is applied to each individual file to reduce noise and remove background, i.e., unwanted signals that could compromise the quality of the

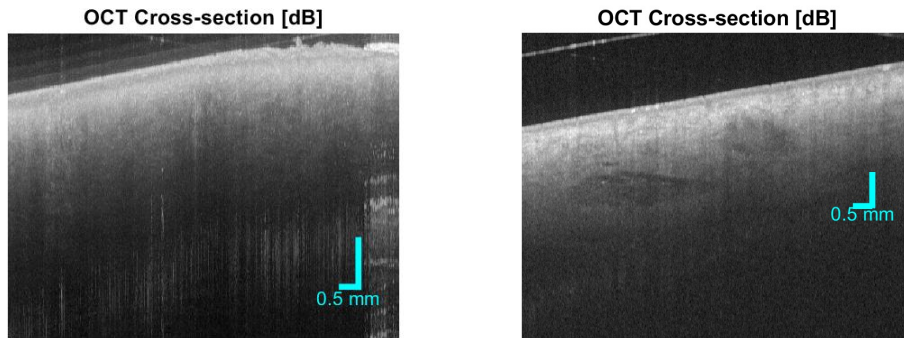


Figure 2.3: *Of the same acquisition, a cross-section obtained with an inadequate ROI is shown in the first image above. In the second image, the cross-section allows to see all the details instead.*

final image. This is achieved by subtracting from each pixel of a specific depth the value of the average of the pixels in the same row: this operation improves contrast and the representation and visualization of blood vessels, reducing background noise while not repeating the same acquisition several times.

Next, to increase the frequency resolution of the image, the zero-padding technique, which consists of adding zeros to the beginning and end of the data matrix, is applied first. Further improvement is made by windowing accomplished on the data to reduce the effect of distortions and discontinuities that can cause artifacts.

Finally, the Fast Fourier Transform (FFT) is applied: it allows switching from the frequency domain to the space domain and makes it possible to analyze the data by highlighting the most significant structural variations. As a final step, the negative, informatively redundant part of the spectrum is removed to retain only the relevant information for processing.

At this point, the processed data are stored in a complex volumetric matrix that will later compose the final image of the angiographic volume.

2.2.2 OCTA Reconstruction

From the complex matrix obtained as a result of processing the raw data, the OCTA volume is reconstructed through the intensity-based method. With this technique, only the modulus of the FFT is considered, avoiding phase-related problems. This makes it more robust and reliable when the light source is not perfectly stable, limiting sensitivity to noise.

The starting volume is divided into 4 different sub-volumes, each representing an OCT scan obtained at different times. A correction is applied to the last volume as it is misaligned from the others in a B-scan, making sure that all volumes are aligned.

Then, a B-scan (Fig.2.4) and a cross-section (two-dimensional image on the yz plane) (Fig.2.5) of the first subvolume are displayed on a logarithmic scale for an initial qualitative analysis of the collected data.

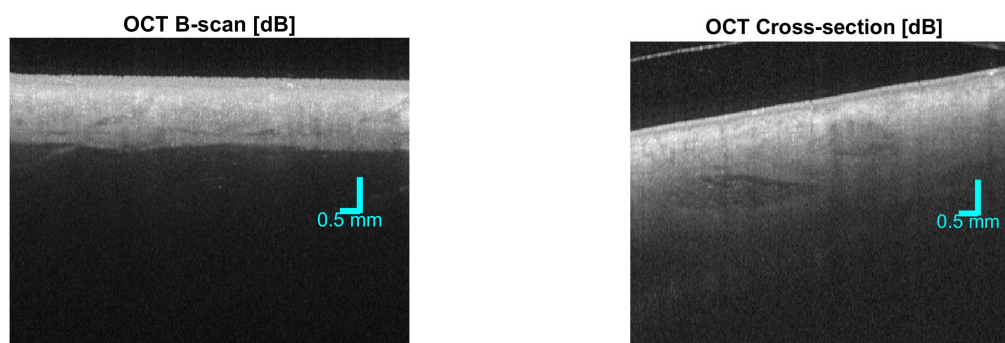


Figure 2.4: *B-scan obtained from an acquisition on the arm, at 8 Newtons.*

Figure 2.5: *Cross-section obtained from an acquisition on the arm, at 8 Newtons.*

The B-scan image shows a cross-section of the skin obtained along a single scan axis. It can be clearly seen that the skin appears as a layered structure: the more reflective surface layer represents the epidermis; in the B-scan, a lighter band can be seen in the upper layer, which can be interpreted as the stratum corneum, i.e., the outermost area. In the cross-section, on the other hand, partly due to the logarithmic scale used, more details of the skin structure and a transition from the more reflective surface to deeper layers are visible.

The epidermis and dermis layers are characterized by different reflectivity: the

dermis, in fact, appears as a darker, and therefore less reflective, area below the epidermis. The transition between epidermis and dermis is usually characterized by a change in signal intensity, and in some areas, the junction between the two layers appears as a darker line between the two regions of different reflectivity.

Blood vessels, on the other hand, appear as dark areas with no signal because the blood itself absorbs and scatters light more than other surrounding tissues. In the cross-section, vascular structures are clearly visible and traceable to the darker, signal-free rounded or elongated areas in the dermis.

At this point, to correctly identify the skin surface within the image and compensate for any slide effects, a median filter is applied to each B-scan. Through an intensity analysis of the pixels that make up the A-scans, pixels that exceed a certain threshold can be identified and interpolated with a linear polynomial curve: this will represent the skin surface line (Fig2.6). Once the surface line is identified for all B-scans, the entire skin section is reconstructed and used to realign the volumes to a horizontal level.

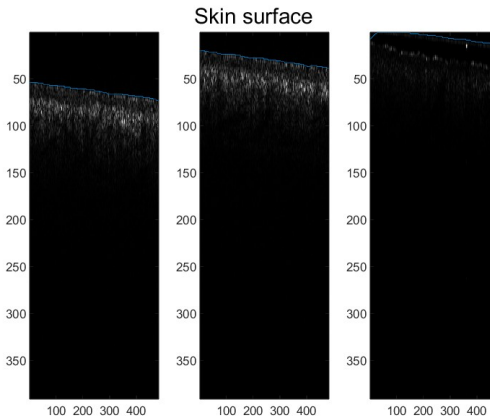


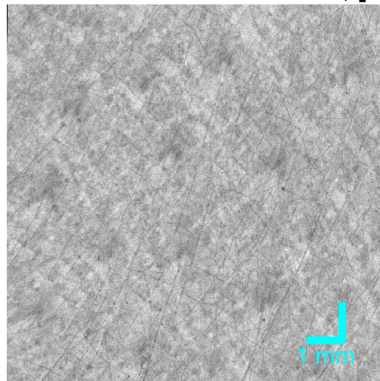
Figure 2.6: *Visualization of the linear fitting (blue line on the surface) used to identify the skin surface.*

Finally, OCTA volume is reconstructed, which is based on the movement of blood flow. Although static structures remain constant between successive acquisitions, blood vessels, on the other hand, show variation in intensity. Therefore, angiography is obtained as the difference between B-scans of the same acquisition, but acquired in sequential time instants, highlighting vascular structures.

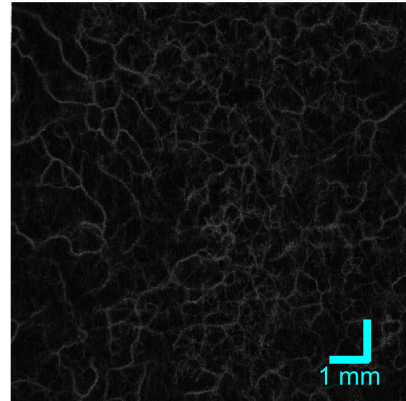
From here it is possible to visualize, as shown in Fig.2.7:

- **OCT en-face:** image view projected along the depth axis, representing one of the four reconstructed OCT volumes.
- **Intensity-Angio en-face:** image showing the vascular structure, obtained from the volumes acquired in sequential time instants.

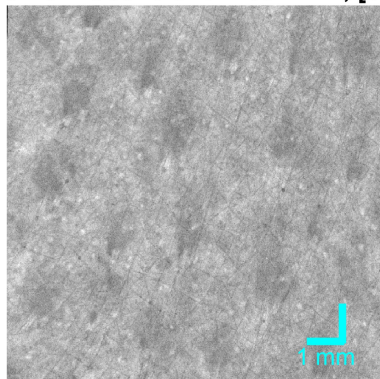
OCT en-face: 0.192-0.575 mm, [dB]



Intensity-Angio, en-face: 0.192-0.575 mm



OCT en-face: 0.575-1.054 mm, [dB]



Intensity-Angio, en-face: 0.575-1.054 mm

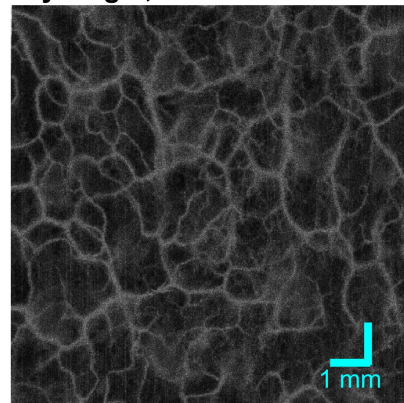


Figure 2.7: OCT en-face and Intensity-Angio en-face at different depths, belonging to an acquisition on the leg.

Also in this study, angiographies were analyzed considering two different depths:

- **Superficial Layer:** 0.192 - 0.575 mm
- **Deep Layer:** 0.575 - 1.054 mm

2.2.3 Artifact Removal

Following the reconstruction of the OCTA volume, the next step is the attenuation of artifacts that compromise its quality, a key requirement to ensure a more accurate and reliable analysis of the data.

The improvement of the final image was achieved by correcting the following artifacts:

- **White Line correction**

This artifact can be caused by multiple factors. The first of these relates to involuntary movements made by the volunteer on whom the acquisition is being performed; in addition, breathing and heartbeat can also introduce minimal movements that, however, can affect the quality of the collected data. In addition, a change in OCT laser power during acquisition can also generate artifacts. For correction, a normalization is performed on each B-scan against the average of all acquired B-scans, equalizing the intensity and reducing the differences between lighter and darker regions. Since this artifact causes considerable variations in intensity (white lines) in the image, division by the mean helps to reduce its effect, making the image more uniform and homogeneous.

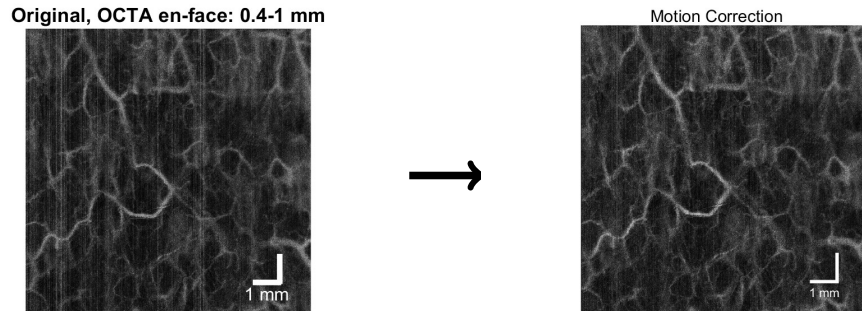


Figure 2.8: *Original OCTA image (left) and image after white line correction (right), in an acquisition on the leg at 4 Newtons.*

- **Projection artifact**

This artifact occurs when the image of superficial blood vessels is projected onto the underlying layers, incorrectly resulting in the visualization of vascular structures not actually present in those layers.

When light from the OCT system is reflected by red blood cells, the presence of blood vessels is identified. However, once this light is partially changed by passage through the bloodstream, it can be reflected back to the OCT and recorded as a signal. Since the signal varies over time, the OCTA interprets it as blood flow even in the deeper layers, so the image will appear as if it is counting blood vessels with the pattern of overlying vessels[34].

To correct for projection artifacts, exponential filtering is applied: the intensity of each pixel in the image is updated by multiplying it by an exponential gamma factor, which depends on the previous values in the same column. In this way, a progressive dimming effect of pixel intensity occurs, reducing artifacts from the upper layers.

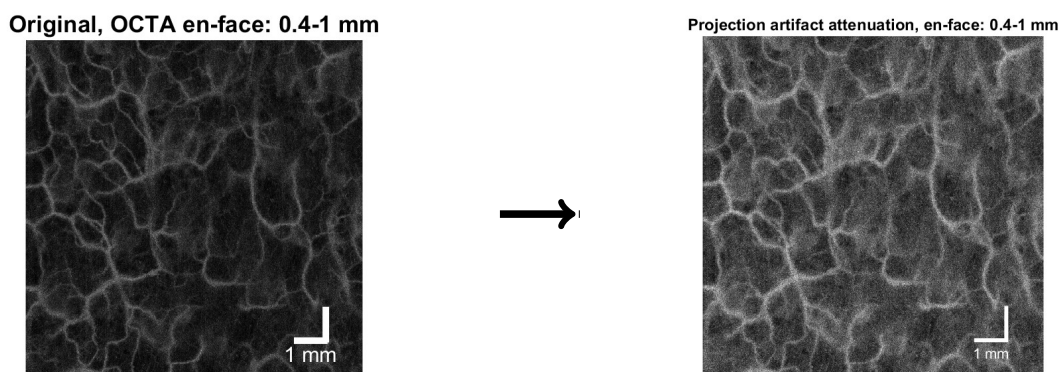


Figure 2.9: *Original OCTA image (left) and image after projection artifact correction (right), in an acquisition on the arm at 4 Newtons.*

- **Smoothing filter**

A 3D median filter is applied to reduce noise and residual artifacts. This is a filter that is not convolutional but acts locally using a three-dimensional kernel of size 3x3x3: the window values are sorted in ascending order and the center pixel is replaced with the median value of the pixels in the window. In this way, the image details are not blurred but the impulsive noise, so-called salt-and-pepper noise, which strongly affects the dataset, is attenuated.

- **Contrast enhancement**

As a final step, to improve the quality of the OCTA image, the contrast is affected. Specifically, in this study, the average brightness of all pixels is calculated and then all pixels in the image are scanned: if it is lighter than average, then its intensity is increased; conversely, if it is darker than average, its intensity is decreased. Overall, the contrast between light and dark areas of the image is increased, but the average is kept the same, balancing the increase and decrease in intensity of each pixel.

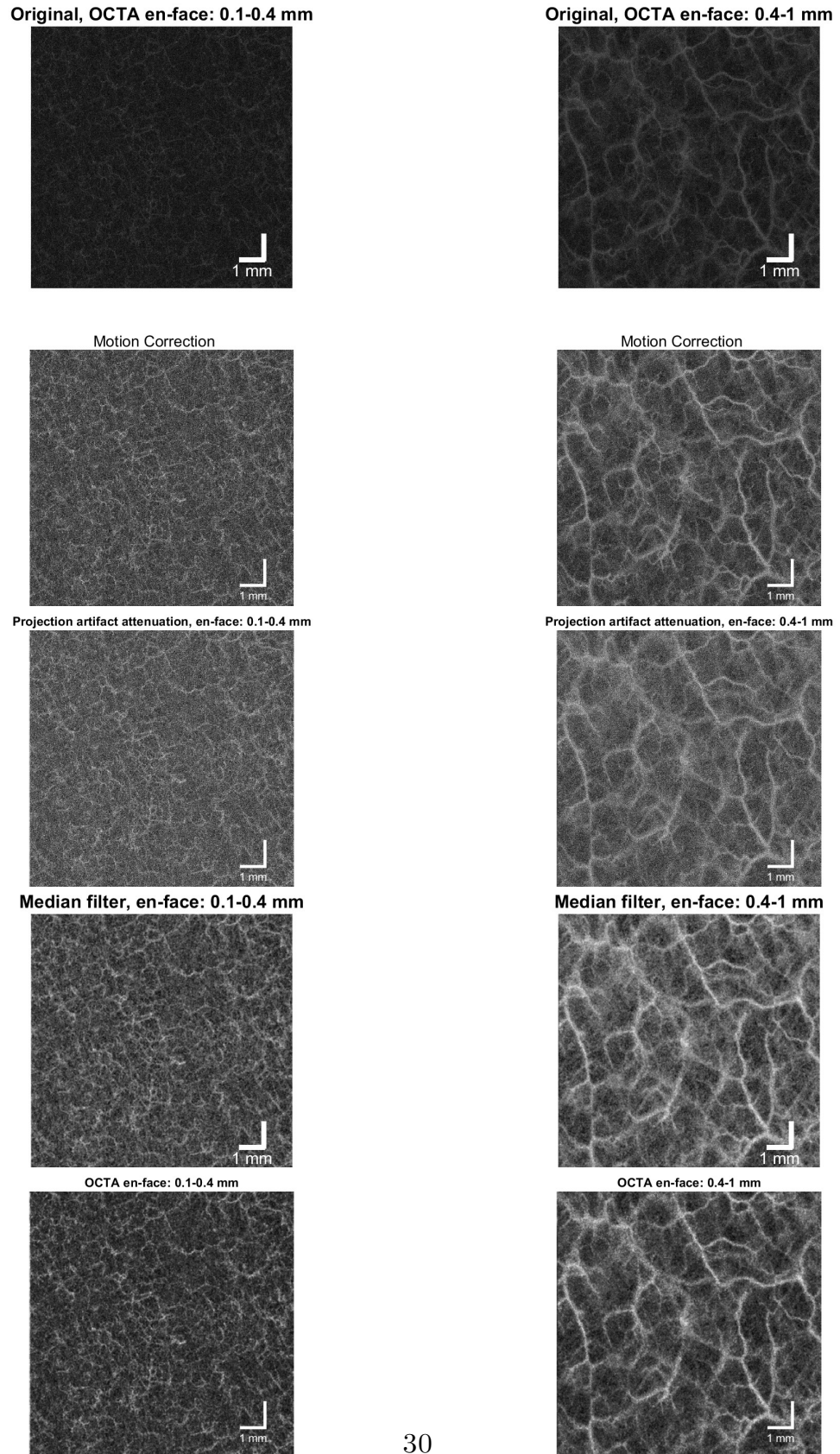


Figure 2.10: Representation of the artifact removal pipeline in the 2 layers, superficial (left coloumn) and deep (right coloumn).

2.3 Evaluation Metrics

Understanding the relationship between the pressure applied by the probe and the quality of the angiographic image is critical to obtaining accurate, reproducible, and, as an ultimate goal, clinically reliable acquisitions. This aspect is also particularly relevant from a diagnostic point of view, since variations in the pressure applied can significantly affect image quality, altering the visibility and definition of vascular structures.

In some cases, the structural features of an image can be qualitatively assessed by visual analysis. However, this approach is subjective and dependent on the experience of the observer. Instead, in order to have a more objective and reproducible assessment, it is often necessary to use quantitative methods supported by automated analysis algorithms.

After applying the Artifact removal pipeline to the reconstructed OCTA volumes, it is essential to continue the analysis to determine how the pressure exerted by the OCT system probe affects the final image quality. To this end, we proceed with evaluation using image quality metrics and texture parameters to quantify the impact of pressure on vascular detail definition, contrast, and the presence of artifacts.

Through the use of appropriate evaluation metrics, it will be possible to establish optimal pressure thresholds that ensure standardized acquisitions of appropriate quality, thereby improving the reliability of OCTA images for both research and clinical application.

The metrics considered in this study are:

- **Mean Noise Level**
- **PSNR** (Peak Signal-to-Noise Ratio)
- **BRISQUE**
- **NIQE**
- **PIQE**
- **Entropy**
- **Skewness**
- **Vascular Density**

2.3.1 Noise parameters: Mean Noise Level and PSNR

Mean Noise Level is a metric used to quantify the amount of residual noise present in the OCTA volume following the artifact correction process. It is calculated by comparing the original raw volume with the volume processed through the artifact removal pipeline: the difference between the two volumes allows us to estimate the extent to which noise has been attenuated and the amount of remaining noise, if any.

At the same time, the **Peak Signal-to-Noise Ratio (PSNR)** is a parameter used to evaluate image quality, as it measures the ratio of maximum signal power to noise power. Its calculation is based on measuring the mean square error (MSE) between the original and the processed image, and then converted to a logarithmic scale. The MSE quantifies the average of the squared differences between the corresponding pixels of the two images: low MSE values indicate greater similarity between the images, while higher values suggest the presence of distortions.

The equation for PSNR is:

$$\text{PSNR} = 10 \log_{10} \left(\frac{I_{\max}^2}{\text{MSE}(I, \hat{I})} \right) \quad (2.1)$$

where I is the raw image, \hat{I} is the processed image, and I_{\max} is the maximum intensity value in the raw image [35].

A high PSNR value indicates better image quality, with optimal signal-to-noise ratio and fewer artifacts. In contrast, a low PSNR value suggests that noise or artifacts introduced by the acquisition or processing process compromise image quality.

The combined analysis of these two noise-related metrics is employed to estimate the effect of probe pressure on OCTA image quality. Indeed, variations in pressure can affect the contact between the probe and the skin surface, altering the level of noise present in the acquired volumes.

Too low a contact pressure, in fact, could reduce image quality due to less adhesion between the probe and the skin, with possible artifacts resulting from suboptimal signal reflection. Conversely, too much pressure could cause tissue deformation and alter local blood perfusion, affecting image quality [35], [36].

2.3.2 Image Quality metrics

BRISQUE, **NIQE** and **PIQE** are Matlab metrics used to evaluate the quality of images. The main characteristic of these algorithms lies in the fact that they operate without comparing the analyzed image with a hypothetical original reference image. For this reason, they are particularly suitable in this study, since a distortion-free reference image is not available. Each of these three metrics performs visual image quality analysis in different ways, with different calculation methods and levels of correspondence to human perception.

BRISQUE (Blind/Referenceless Image Spatial Quality Evaluator) is based on a model trained with images containing known distortions and subjective assessments of visual quality. This provides estimates that often accurately reflect human perception. However, since this metric is trained on a specific set of distortions, its effectiveness may be reduced if it is applied to images with different artifacts than those in its training database.

In contrast to **BRISQUE**, **NIQE** (Natural Image Quality Evaluator) does not make use of subjective evaluations. Its model is based exclusively on high-quality images without distortions, known as “pristine images,” so it is more versatile and applicable to a wide range of images with different alterations. However, precisely because it does not take into account the subjective perception of quality, its results may sometimes deviate from human judgment.

Finally, **PIQE** (Perception-based Image Quality Evaluator) adopts an even different method of analysis. It does not require a pre-trained model, like the other two previous metrics, and is capable of evaluating image quality on its own. The calculation method used is based on dividing the image into smaller areas, where the level of distortion is evaluated according to the local variation in details. This feature makes it extremely flexible and suitable for different types of images, without the need for a training phase.

In OCTA image analysis, these image-quality metrics play a key role in assessing the impact of probe pressure on acquisition quality. **BRISQUE** is particularly useful in estimating how much the perceived image quality is compromised by the presence of artifacts due to suboptimal pressure. If excessive or insufficient probe pressure introduces distortions similar to those already present in the metric training database, **BRISQUE** can provide a reliable indication of actual quality degradation. **NIQE** analyzes image quality based on statistical models of undistorted images: changes in pressure that can alter contrast or noise distribution can be detected by this metric as a reduction in quality. Finally, **PIQE**, because of its feature of

assessing distortion locally, is particularly useful in identifying specific regions of the image where the signal is compromised by suboptimal probe-skin contact.

2.3.3 Texture metrics

In this study, in addition, entropy and skewness parameters were calculated to evaluate the structural and statistical characteristics of OCTA images in relation to the pressure applied by the probe.

Entropy is a measure of the complexity and level of information contained in an image. A high value indicates greater variability in intensity levels, typical of an image with a more complex and detailed structure. In the OCTA images analyzed, entropy can be affected by variations in probe pressure: too little pressure could reduce the contrast between the blood vessels and the surrounding tissue, decreasing the amount of detectable information, while too much pressure could cause artifacts that alter the intensity distribution, leading to an erroneous increase in image complexity. Entropy is calculated through the probability distribution of image intensity levels, according to the following formula:

$$H = - \sum_i p(i) \log_2 p(i) \quad (2.2)$$

where $p(i)$ represents the probability of occurrence of intensity i in the image.

Skewness is a statistical measure that describes the distribution of image intensity levels relative to their mean. A positive skewness value indicates a greater presence of pixels with lower than average intensities, while a negative value suggests a greater concentration of pixels with higher intensities. In OCTA images, probe pressure can affect the distribution of light intensity, changing the skewness value of the image. For example, excessive pressure could compress tissues and alter blood perfusion, changing reflectance levels and causing skewness variation in pixel distribution. Skewness is calculated as:

$$S = \frac{1}{N} \sum_i \left(\frac{x_i - \mu}{\sigma} \right)^3 \quad (2.3)$$

where x_i are the pixel intensity values, μ is the mean, σ the standard deviation, and N the total number of pixels in the image.

Analysis of these parameters provides insight into how probe pressure affects not only the visual quality of the image, but also its statistical and structural

properties, providing additional information to obtain more reliable OCTA images that are representative of the real vasculature.

2.3.4 Vascular Density

Vascular density is a morphological parameter that allows, in this study, to assess the impact of probe pressure on OCTA images.

This metric represents the proportion of blood vessels detected in the image to the total area, and is characterized as a key indicator for assessing vascular perfusion at different pressure levels. Specifically, in this study, vascular density is defined as the ratio of the total number of pixels belonging to the vascular skeleton to the total number of pixels in the image:

$$VD = \frac{\sum_i P_{\text{skeleton}}(i)}{N_{\text{total}}} \quad (2.4)$$

where VD indicates vascular density, while the numerator represents the number of pixels that make up the skeletonized structure of the vessels, and N_{total} is the total number of pixels in the image.

Probe pressure can significantly affect the measurement of vascular density. If the applied pressure is too high, it could compress the underlying tissues, temporarily reducing local blood flow and causing an underestimation of vascular density. Conversely, too little pressure could impair the quality of the recorded signal, reducing the contrast between the vessels and the surrounding tissue and leading to misidentification of the vascular structure.

Analysis of superficial and deep vascular density allows us to assess how probe pressure affects different layers of the vasculature differently. While superficial vessels may be more susceptible to pressure changes because of their proximity to the skin surface, deep vessels, on the other hand, may be affected more markedly by tissue compression. This analysis provides important information for optimizing acquisition conditions to obtain reliable and representative OCTA images of microvascular perfusion.

2.3.5 Computation of metrics

In this thesis work, evaluation metrics were calculated at different levels of analysis of the dataset, however, the division between superficial and deep layers, corresponding to different levels of depth of the skin structure, remains constant.

Mean Noise Level and PSNR metrics were estimated directly on the OCTA volumes, comparing the raw one with the processed one, leading the analysis back to a three-dimensional residual noise estimate.

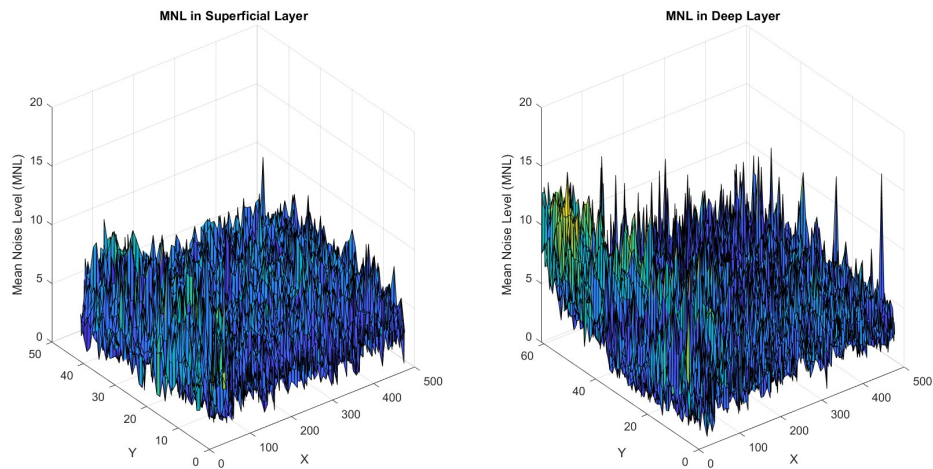


Figure 2.11: 3D graph showing the spatial distribution of Mean Noise Level (MNL) in an acquisition on the arm, in the superficial (left) and deep layer (right).

Subsequently, however, the entire dataset is returned to two-dimensional values through the calculation of Maximum Intensity Projection (MIP). This is a projection technique used in medical image processing to represent three-dimensional data in two dimensions, facilitating visual and quantitative analysis. This method involves selecting, for each pixel in the projection, the average of the pixel intensities along the depth axis. In OCTA images, MIP allows for a two-dimensional representation of vascular structures, emphasizing vessels with higher intensities.

The MIP is normalized between 0 and 1 before calculating image quality metrics (BRISQUE, NIQE and PIQE) in order to make the results comparable between different body regions. In addition, normalization made it possible to eliminate scaling differences due to absolute intensity variations between images, improving the reliability of quantitative comparisons.

In contrast, however, for the calculation of the entropy and skewness parameters, normalization was adopted with respect to the maximum values of the entire dataset. This approach avoids that images with higher intensity levels suffered penalties due to noise amplification, thus a more stable and comparable analysis across acquisitions is ensured.

MIP imaging provides a summarized view of vascular structure, making it easier to assess image quality and structural properties. However, this technique can result in a loss of information on vessel depth, so it has been used in combination with other metrics to achieve a more comprehensive analysis.

Vascular density was calculated in two ways: either directly on the binarized image or on the OCTA image skeleton. In the first case, from the MIP, the image mask was calculated by adaptive binarization, which assigns variable thresholds based on the local intensity distribution. In the second case, after a preliminary filtering step to reduce noise, a Top-Hat transformation was applied to make vascular structures more visible, followed by an adaptive binarization. Next, through morphological operations, the continuity of the vascular network was improved. Finally, skeletonization was performed with the *bwskel* and *bwmorph* operators, removing smaller branches and improving the connectivity of the microvascular network. The result of these operations is shown in fig.2.12.

The combined use of these techniques made it possible to assess the impact of probe pressure not only on image quality, but also on vascular density metrics and structural properties of OCTA images, providing a more in-depth and reliable view of the phenomenon analyzed.

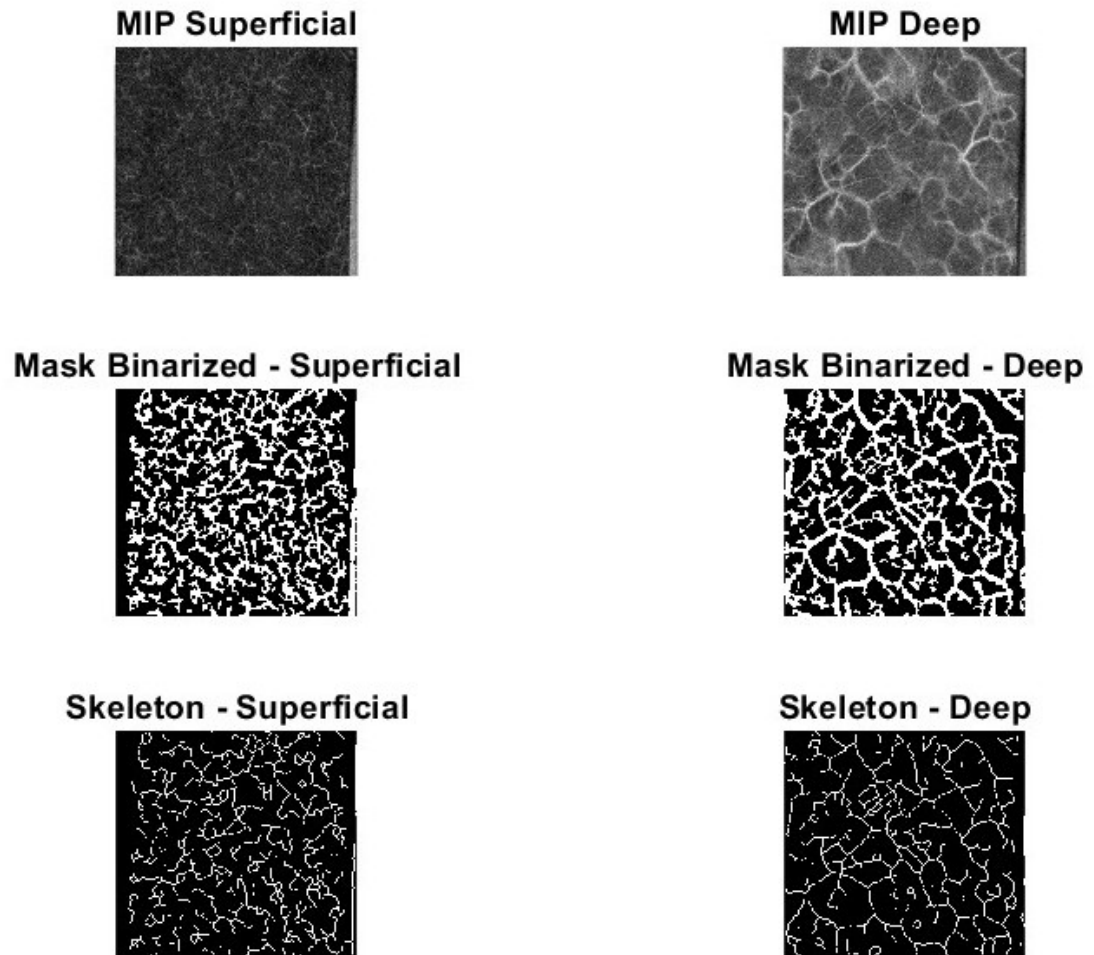


Figure 2.12: *From top to bottom: MIP, binarized image and skeleton of an OCTA volume acquired on the leg at 6 Newtons. The two columns refer to the two analyzed layers, superficial and deep.*

Chapter 3

Results

This chapter shows the results obtained by statistical analysis of metrics extracted previously from OCTA images, with the aim of evaluating the influence of acquisition probe pressure on the quality of angiographic images.

Different statistical tests were performed in order to have a complete evaluation of the entire dataset.

The first test conducted in this study is simple **linear regression**. This is a mathematical model that describes the relationship between an independent variable (X), and a dependent variable (Y).

Regression tries to find a straight line of the shape:

$$Y = \beta_0 + \beta_1 X$$

where:

- Y : Examined metric (dependent variable)
- X : Pressure (independent variable)
- β_0 : Intercept (value of Y when $X = 0$)
- β_1 : Slope coefficient (how much Y increases for each unit of X)

The goal of linear regression is to find the values of β_0 and β_1 that best describe the relationship between X and Y . The Matlab function used to find the regression line is `fitlm` (Fit Linear Model): this function, in fact, internally performs the least squares method, which minimizes the error between the actual values and those predicted by the regression model. After creating the linear model and finding

the regression line, the β_1 values for each parameter are evaluated to identify the statistically significant values, that is, the parameters with $pvalue < 0.05$. This indicates that the effect of pressure on the metric of interest is significant with an error probability of less than 5%.

An initial linear regression was performed on the entire dataset, keeping the division between surface and deep layer only. The regression results are shown in Fig. 3.3 for superficial layer and in Fig. 3.4 for deep layer.

The statistically significant metrics ($pvalue < 0.05$) for the superficial layer are:

- Mean Noise Level: -6.28%
- PSNR: $+1.22\%$
- Skewness: $+5.11\%$

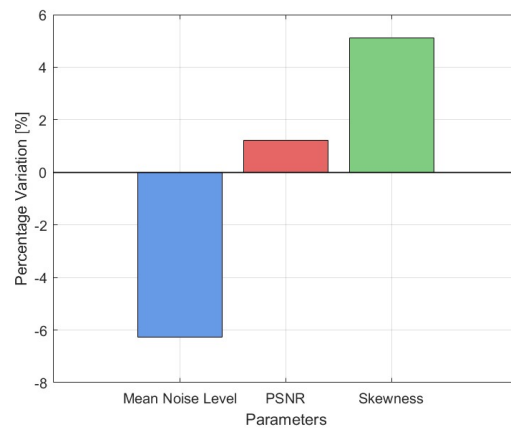


Figure 3.1: Significant metrics visualization for superficial layer.

The statistically significant metrics ($pvalue < 0.05$) for the deep layer are:

- Mean Noise Level: -3.08%
- PSNR: $+0.74\%$

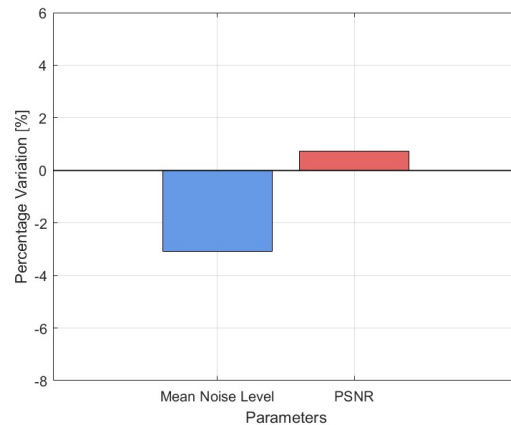


Figure 3.2: Significant metrics visualization for deep layer.

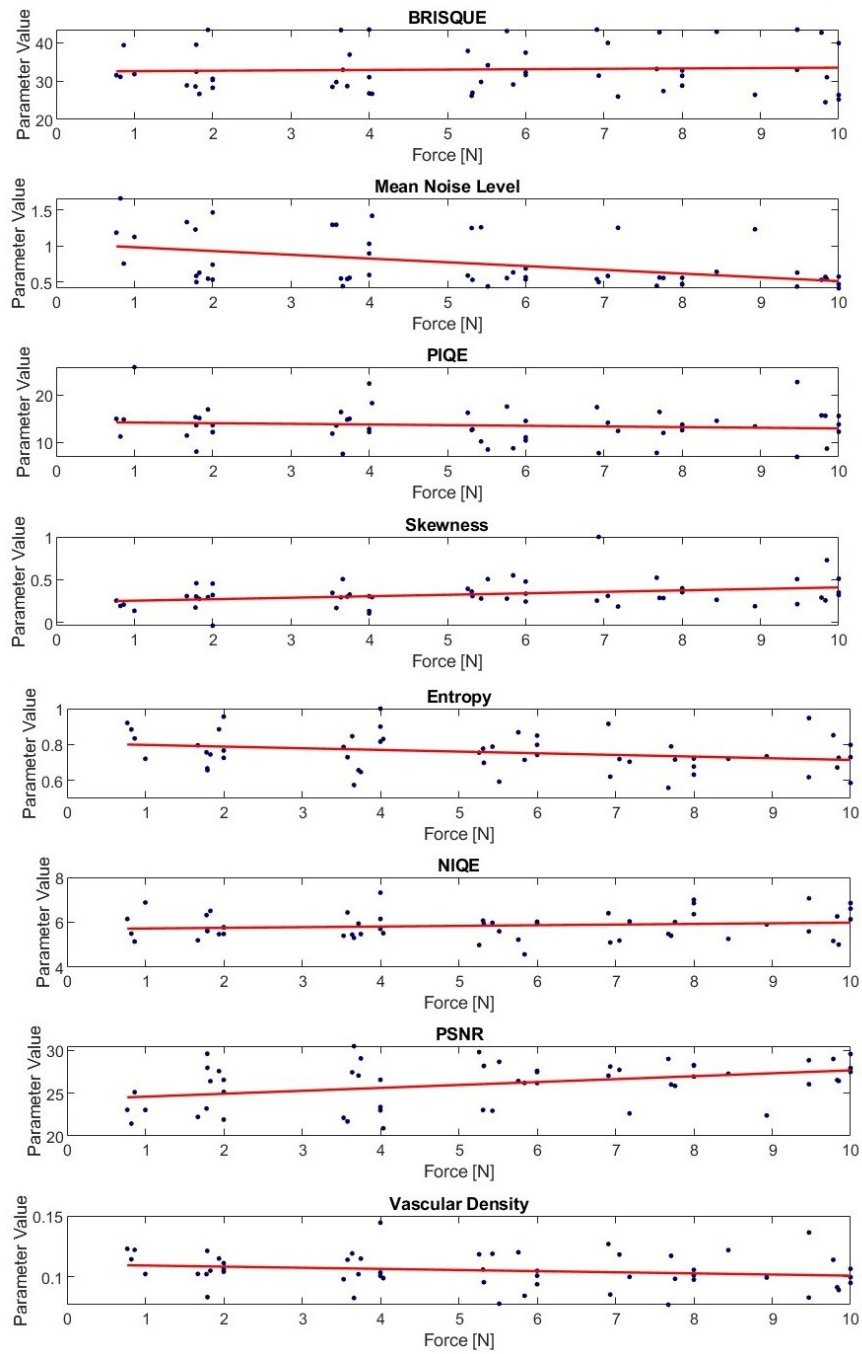


Figure 3.3: Linear regression result for superficial layer.

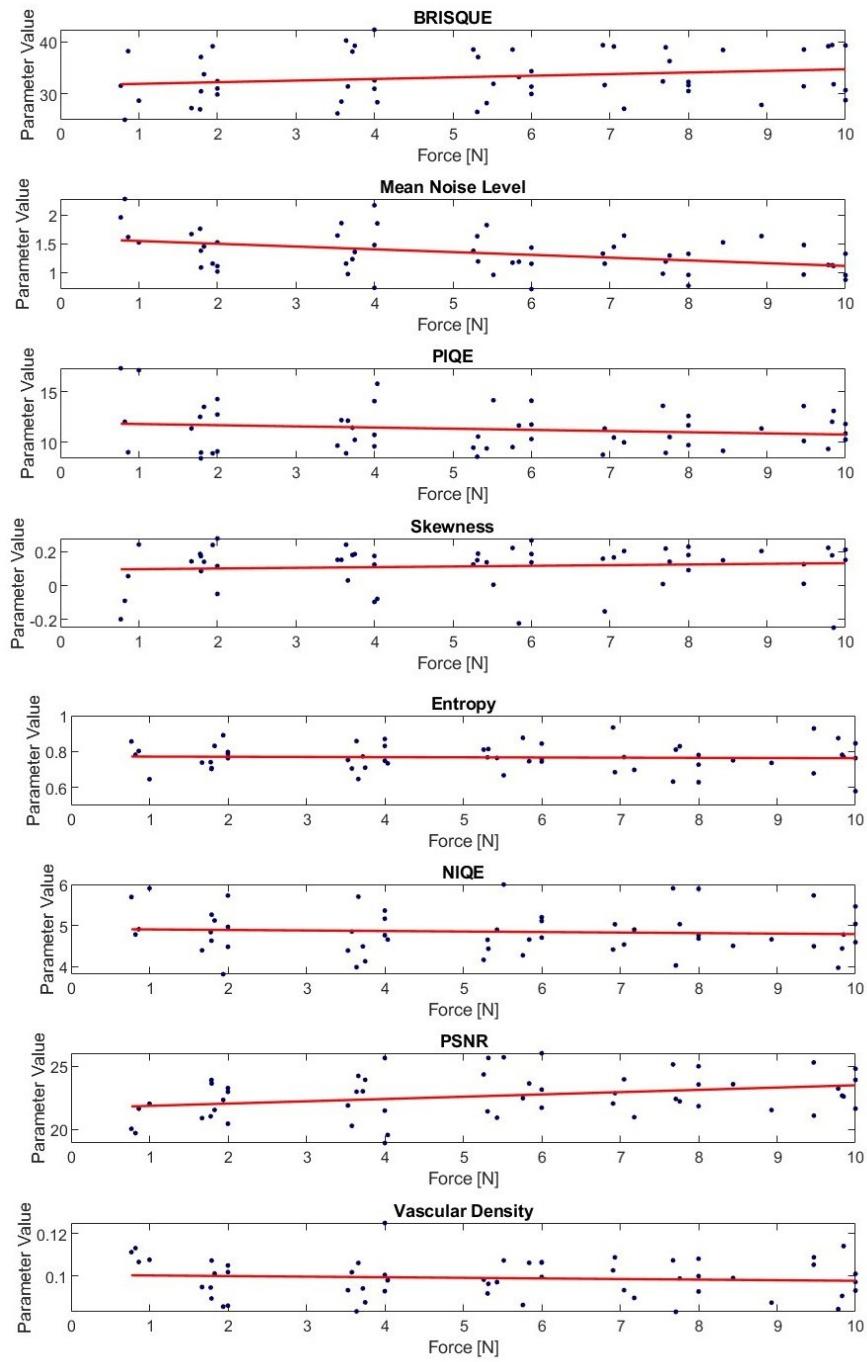


Figure 3.4: Linear regression result for deep layer.

To also include information regarding the analyzed anatomical region, a second linear regression was performed. The entire dataset was divided by layer (superficial and deep) and by anatomical area analyzed (arm, head and leg). This allows obtaining specific regression coefficients for each area-layer-parameter combination instead of a single global regression.

The statistically significant metrics ($pvalue < 0.05$) for each area-layer are:

- **Arm Superficial** (Fig.3.5):
 - BRISQUE: +3.84%
- **Arm Deep** (Fig.3.6):
 - BRISQUE: +2.59%
 - Entropy: +1.69%
- **Head Superficial**(Fig.3.7)
 - Entropy: -3.14%
 - Mean Noise Level: -9.35%
 - PIQE: -6.60%
 - PSNR: +1.85%
 - Skewness: +10.22%
 - Vascular Density (Skeleton): -2.94%
- **Head Deep** (Fig.3.8):
 - Mean Noise Level: -6.20%
 - PSNR: +1.55%
 - Entropy: -1.71%
- **Leg Superficial** (Fig.3.9):
 - Entropy: -1.74%

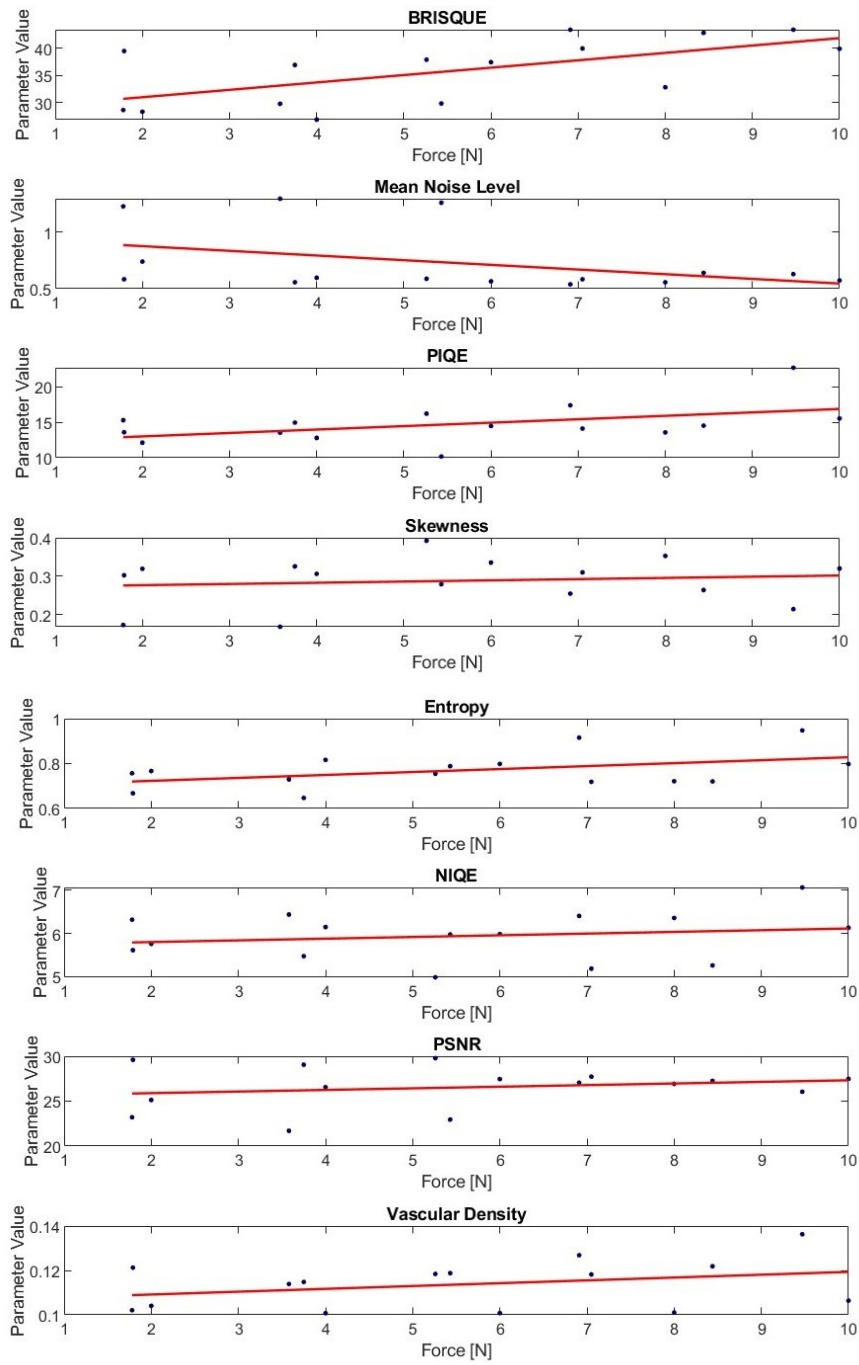


Figure 3.5: Linear regression result for arm superficial layer.

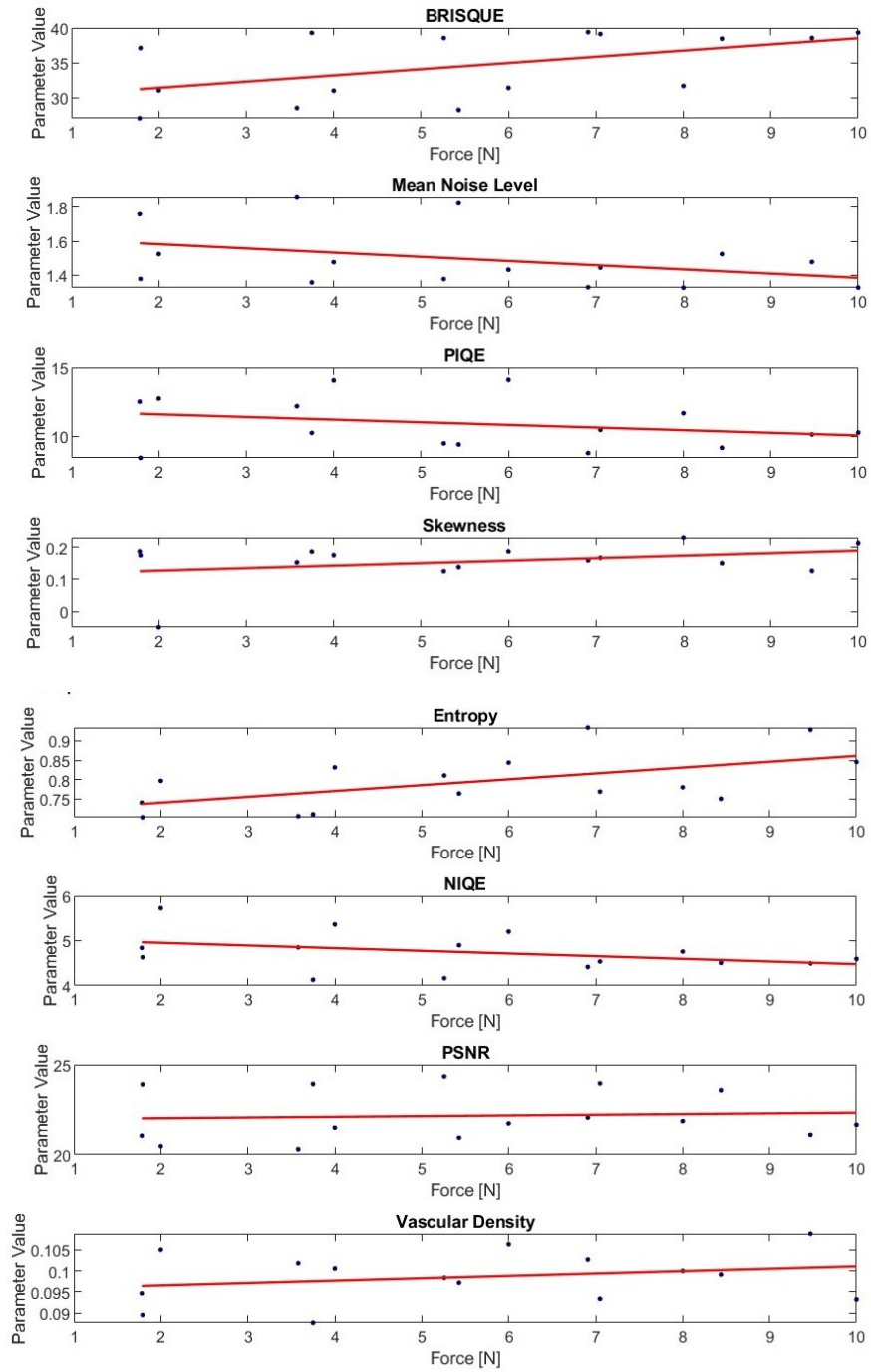


Figure 3.6: Linear regression result for arm deep layer.

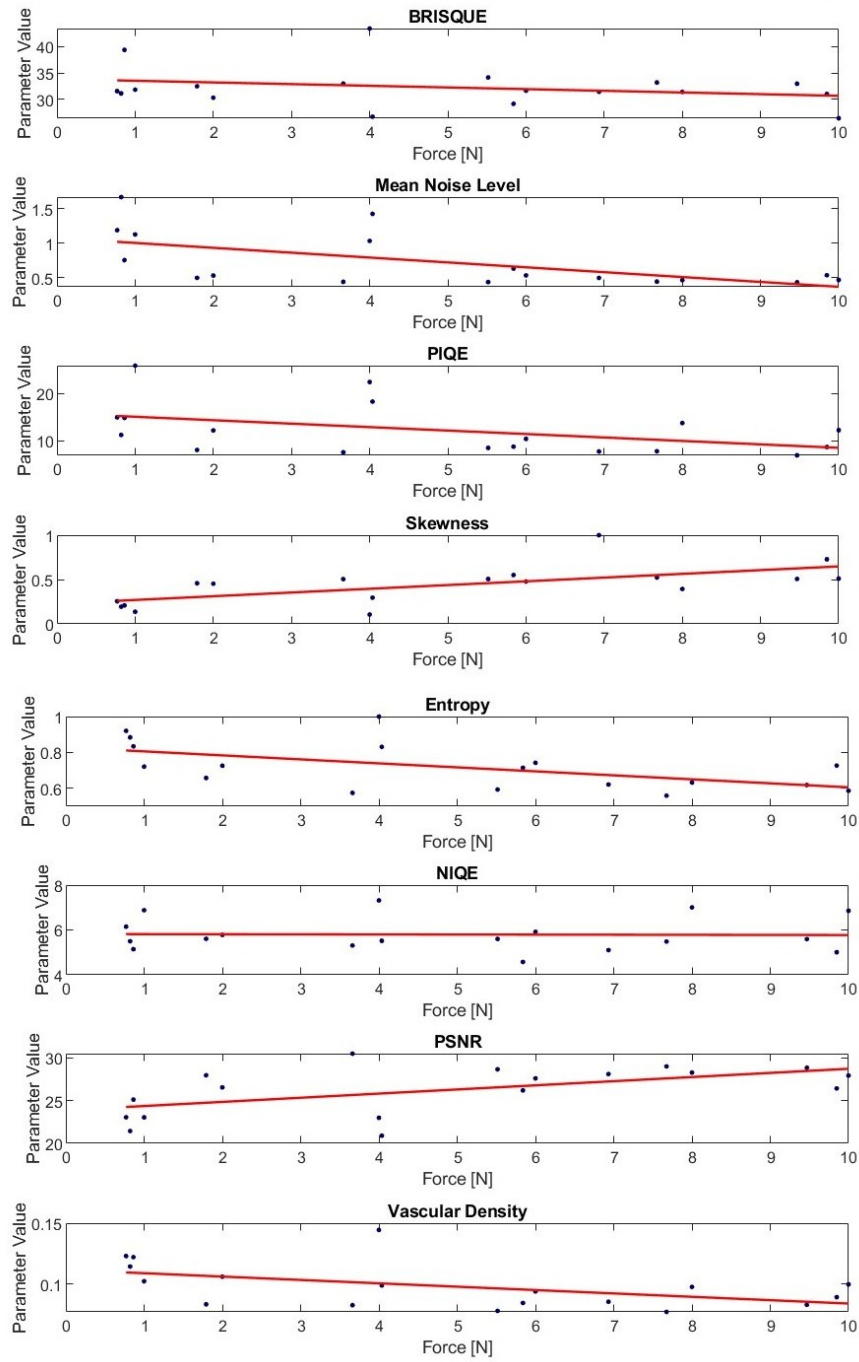


Figure 3.7: Linear regression result for head superficial layer.

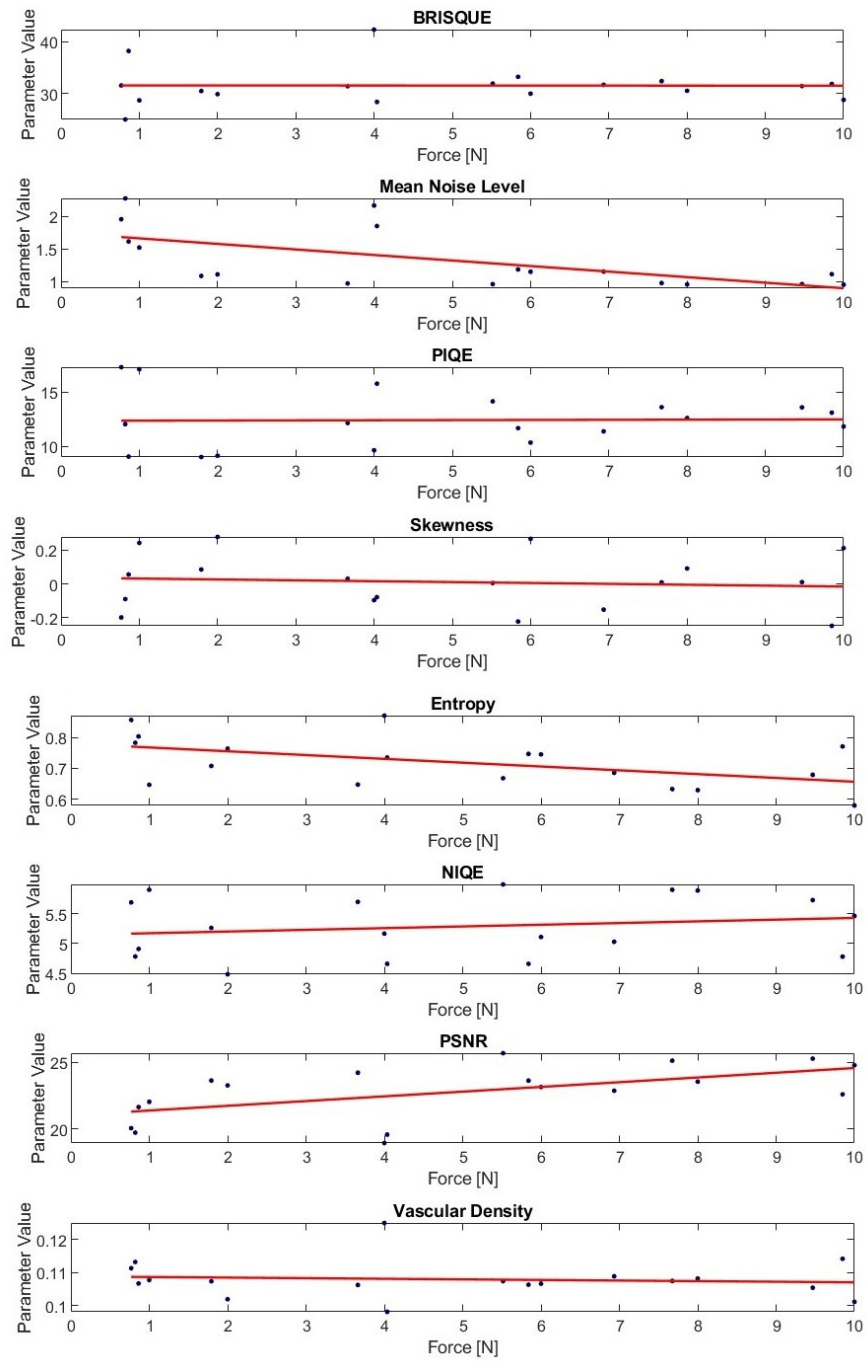


Figure 3.8: Linear regression result for head deep layer.

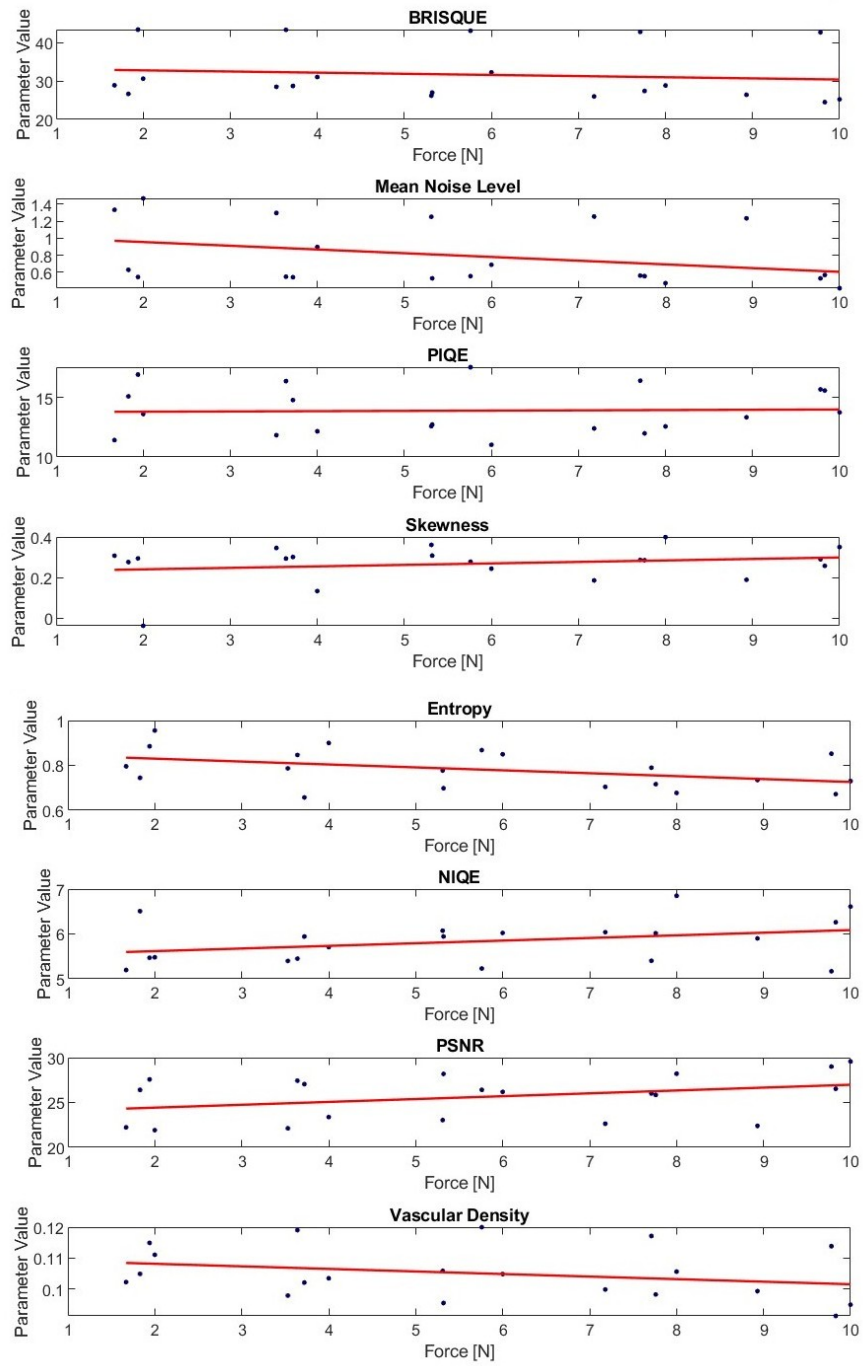


Figure 3.9: Linear regression result for leg superficial layer.

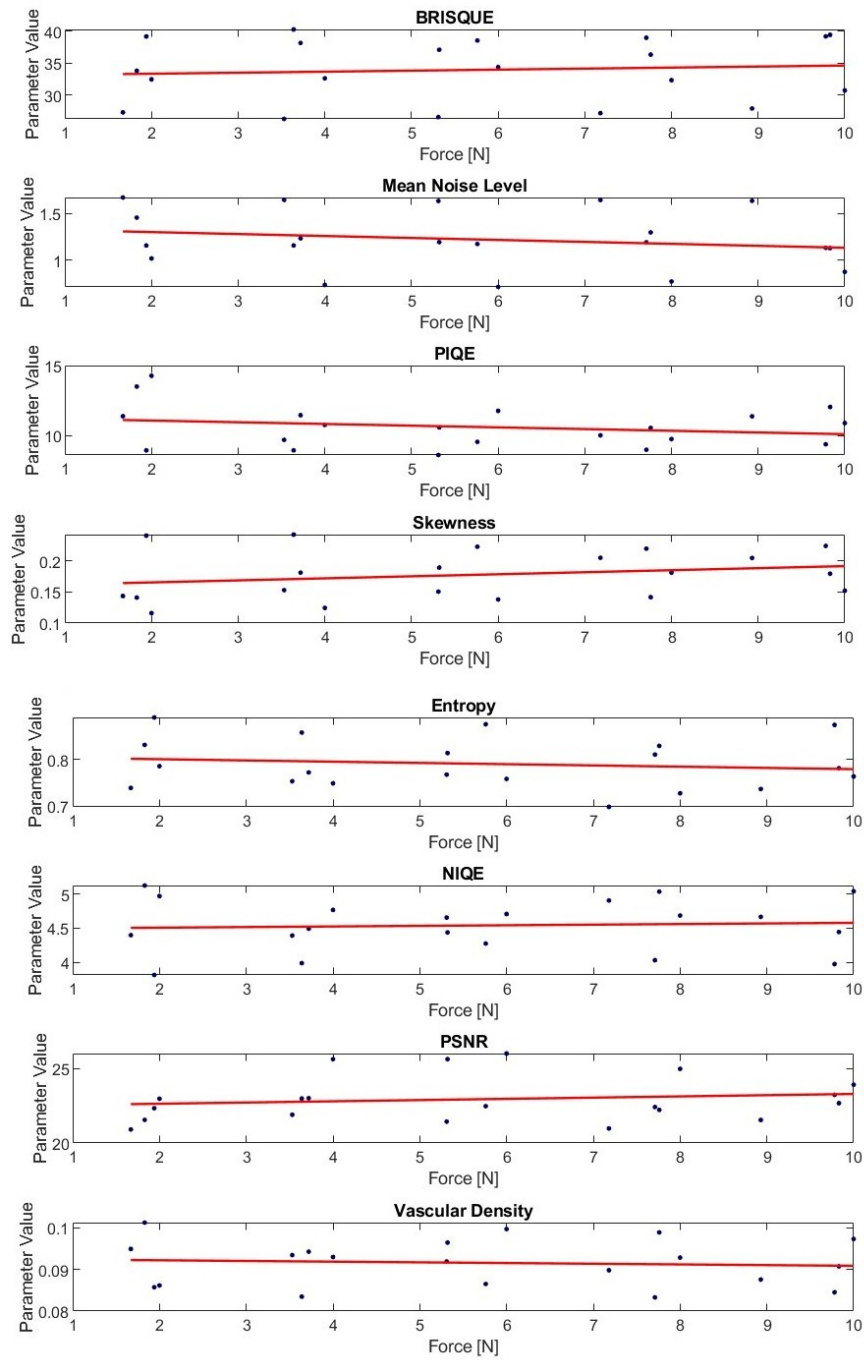


Figure 3.10: Linear regression result for leg deep layer.

To evaluate the presence of statistically significant differences between the groups analyzed, a **one-way ANOVA** (ANalysis Of VAriance) test was performed, a statistical methods for comparing the means of more than two groups.

This test examines how well at least one of the groups has a significantly different mean from the others, using the ratio of the between-group variance to the within-group variance. The null hypothesis (H0) assumes that there are no differences between the averages of the groups, while the alternative hypothesis (HA) holds that at least one group differs from the others.

The ANOVA test returns an F-statistic value, which, when associated with a p-value less than 0.05, indicates that the differences between the groups are statistically significant. However, the ANOVA does not specify which groups are different from each other, which is why a Tukey's Honest Significant Difference Test (**Tukey's post-hoc test**) was performed.

This test allows all pairs of groups to be compared, identifying which differences are statistically significant by calculating specific p-values. In this study, the ANOVA test was applied to compare the averages of the analyzed parameters between different body areas. In cases where the test was significant ($p < 0.05$), Tukey's test made it possible to determine exactly which areas had significant differences between them, providing a more detailed picture of the variability of the parameters considered.

Metrics that showed a significant difference in the ANOVA test ($p_{ANOVA} < 0.05$) are:

BRISQUE ($p_{ANOVA} = 0.0282$)

Tukey's post-hoc test:

- Arm vs Head: $p = 0.024465$ (**significant**)
- Arm vs Leg: $p = 0.1443$ (not significant)
- Head vs Leg: $p = 0.6125$ (not significant)

Entropy ($p_{ANOVA} = 1.0899e-04$)

Tukey's post-hoc test:

- Arm vs Head: $p = 0.0011552$ (**significant**)
- Arm vs Leg: $p = 0.97476$ (not significant)

- Head vs Leg: $p = 0.00022046$ (**significant**)

Vascular Density (Skeleton) ($p_{\text{ANOVA}} = 0.0282$)

Tukey's post-hoc test:

- Arm vs Head: $p = 0.23584$ (not significant)
- Arm vs Leg: $p = 0.021377$ (**significant**)
- Head vs Leg: $p = 0.60118$ (not significant)

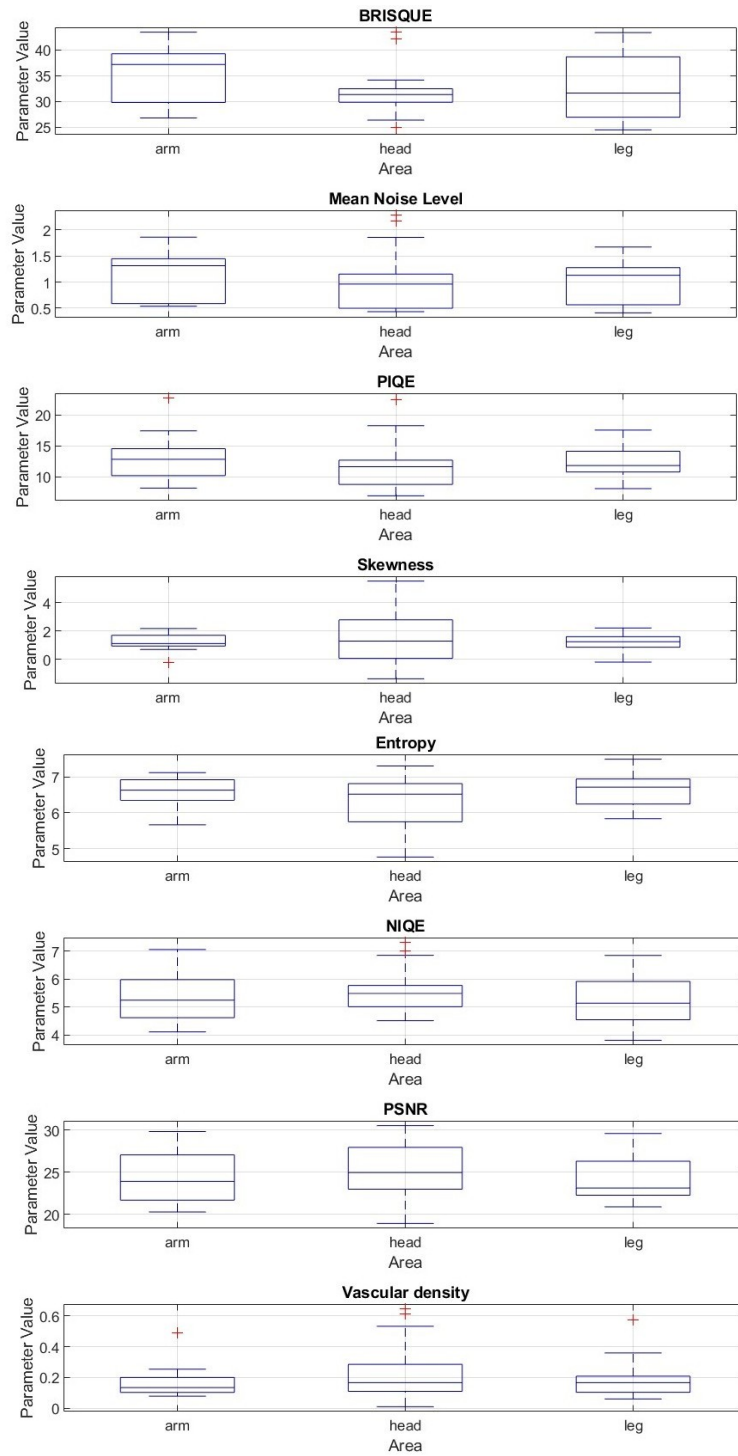


Figure 3.11: *Boxplot of one-way ANOVA test between different body area.*

To estimate the variation of vascular density as a function of pressure in different anatomical regions, its percentage change was calculated. However, to provide a more robust analysis without distortions due to data fluctuations, the calculation was based on a linear regression between vascular density and pressure, rather than on raw values.

The use of linear regression was essential to reduce noise in the data and obtain a more reliable estimation of the relationship between the two variables. If the percentage change had been calculated directly from the raw data, the result could have been affected by random fluctuations or unsystematic variations, making the analysis less reliable. In addition, a calculation based only on the minimum and maximum values of pressure could have introduced bias due to the presence of outliers or the irregular distribution of the data.

Through regression, however, it was possible to model the overall trend of vascular density in relation to pressure. In this way, the influence of local variations is moderated and a more stable and representative measure of the overall trend is obtained. The regression coefficient provides a quantitative indication of the impact of pressure on vascular density, making the results more interpretable and comparable across anatomical conditions.

Finally, the percent change was calculated for vascular density obtained by both binarized mask (Fig.3.12 - 3.13) and skeleton (Fig.3.14 - 3.15), thus enabling a more detailed and complete analysis of structural changes in the vascular network in response to pressure.

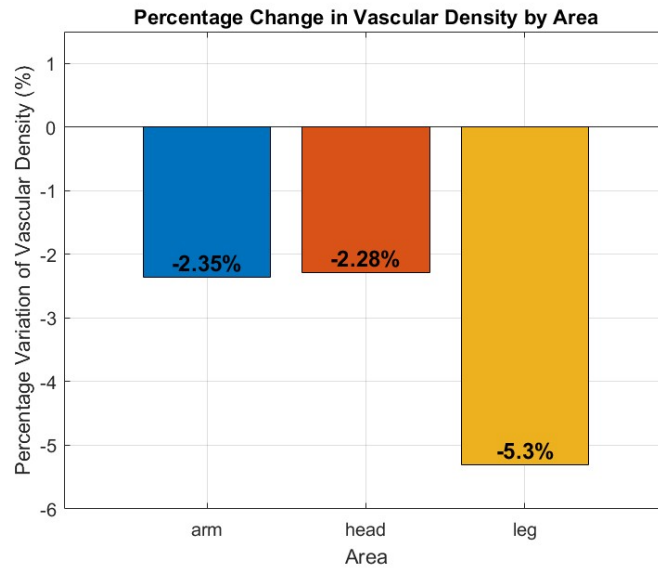


Figure 3.12: Percentage variation in vascular density obtained by binarized mask, in the 3 anatomic regions analyzed.

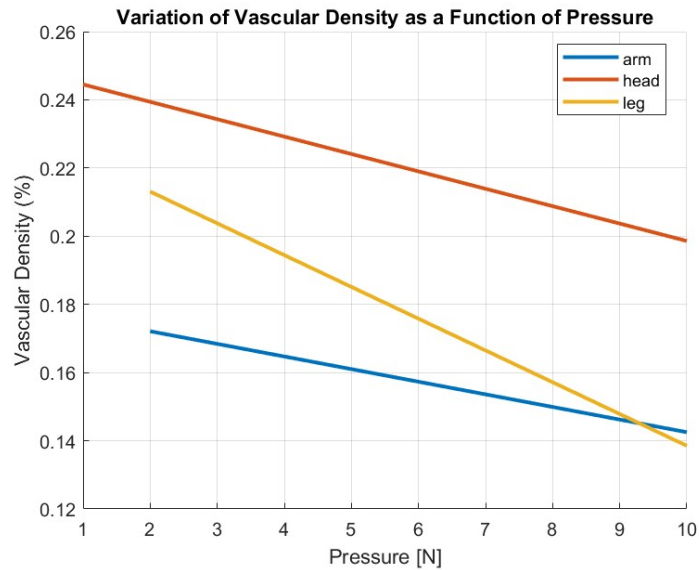


Figure 3.13: Variation in vascular density obtained by binarized mask, in the 3 anatomical regions as a function of pressure.

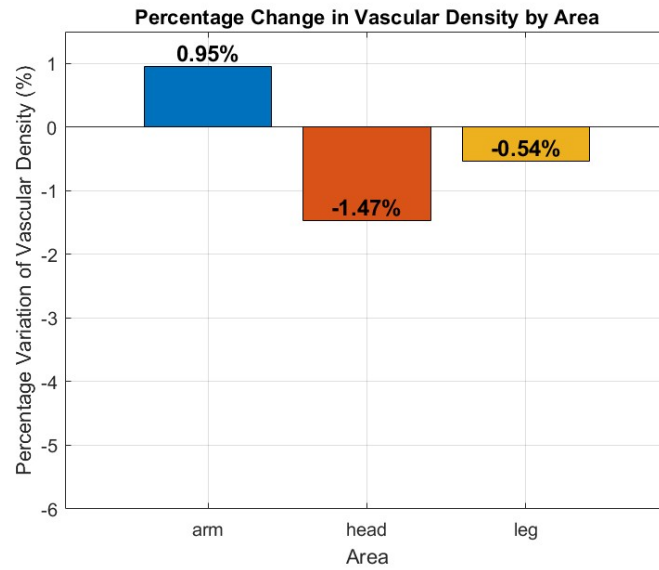


Figure 3.14: Percentage variation in vascular density obtained by skeleton, in the 3 anatomic regions analyzed.

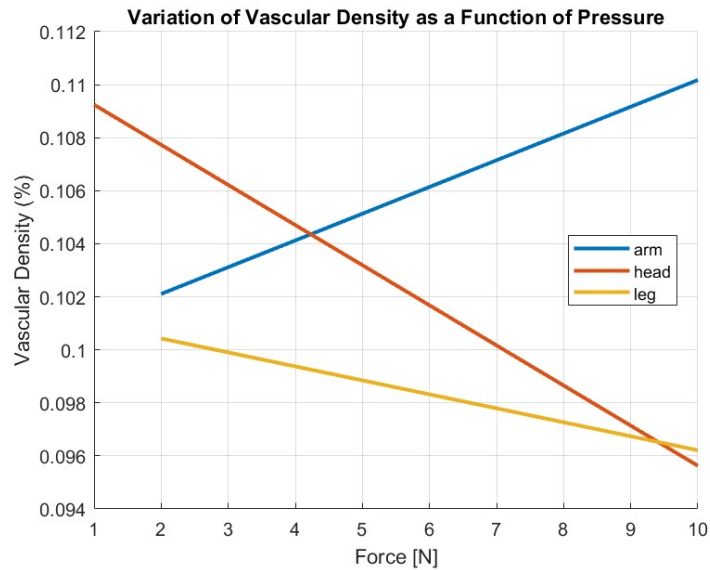


Figure 3.15: Variation in vascular density obtained by skeleton, in the 3 anatomical regions as a function of pressure.

In order to identify the **optimal pressure range** for each body area (head, arm, leg) and for the two layers analyzed (superficial, deep), a code was developed in MATLAB to evaluate the quality of OCTA images in relation to the pressure applied by the probe during acquisition.

In order to obtain reliable results, not all available metrics were considered, but only those that, from the statistical tests performed previously, were found to be significant. Specifically, linear regression analysis showed the significance of **Mean Noise Level**, **PSNR** and **Skewness**, while ANOVA test showed significant differences between body regions for **Vascular Density**, **Entropy** and **BRISQUE**. To provide a uniform comparison between the values of the different metrics, these metrics were subjected to a normalization process.

The optimal pressure range was determined from the calculation of a quality index for each combination of area, layer, and pressure, obtained by averaging the normalized values of the selected metrics. To separate the pressures that produce high quality images, a selection criterium was applied based on the **top 30%** of the quality index. This made it possible to identify the most suitable range of pressures for each area and layer. Finally, the optimal range was defined by considering the minimum and maximum pressure among those included in the selection.

This method makes it possible to determine, for each area and layer, the range of pressures that guarantees high-quality images, avoiding values that are too low, which could increase noise and reduce the visibility of the vascular structure, and pressures that are too high, which could compromise their correct representation.

The result is shown in Tab.3.1

Region	Layer	Min Pressure (N)	Max Pressure (N)
Arm	Superficial	6,91	9,47
Arm	Deep	6,91	9,47
Head	Superficial	0,87	4
Head	Deep	0,87	4
Leg	Superficial	1,94	8,78
Leg	Deep	3,64	5,32

Table 3.1: Optimal pressure range for each anatomical region and layer.

Chapter 4

Discussion

This chapter will discuss the results shown in the previous chapter, obtained from the analysis of the relationship between pressure applied by the OCT system probe and angiographic image quality. The aim is to interpret and examine the results obtained, highlighting their significance and possible implications.

The limitations of the study will also be analyzed, considering the main sources of uncertainty and possible restrictions in the applicability of the results.

4.0.1 Effects of pressure on image quality

The main objective of this thesis is to evaluate the effect of applied probe pressure on OCTA image quality. To this purpose, a simple linear regression analysis was performed, considering the superficial and deep layers separately, to identify a possible relationship between applied pressure and the evaluation metrics analyzed.

The results show that increasing applied pressure results in a reduction of noise in OCTA images. Specifically, pressure has a significant effect on the noise level in both layers. For the surface layer, the reduction in **Mean Noise Level** is particularly marked (-6.28% for each unit increase in pressure). A decrease in noise is also observed in the deep layer, although less pronounced (-3.08%).

PSNR is also found to be affected by increasing the pressure applied during acquisition, with an increase in both layers (+1.22% in the superficial layer and +0.74% in the deep layer), suggesting an improvement in signal-to-noise contrast. This result indicates that a certain level of pressure may be useful in improving image quality by reducing noise and increasing the signal-to-noise ratio. However, excessive pressure could potentially compromise image quality by affecting the

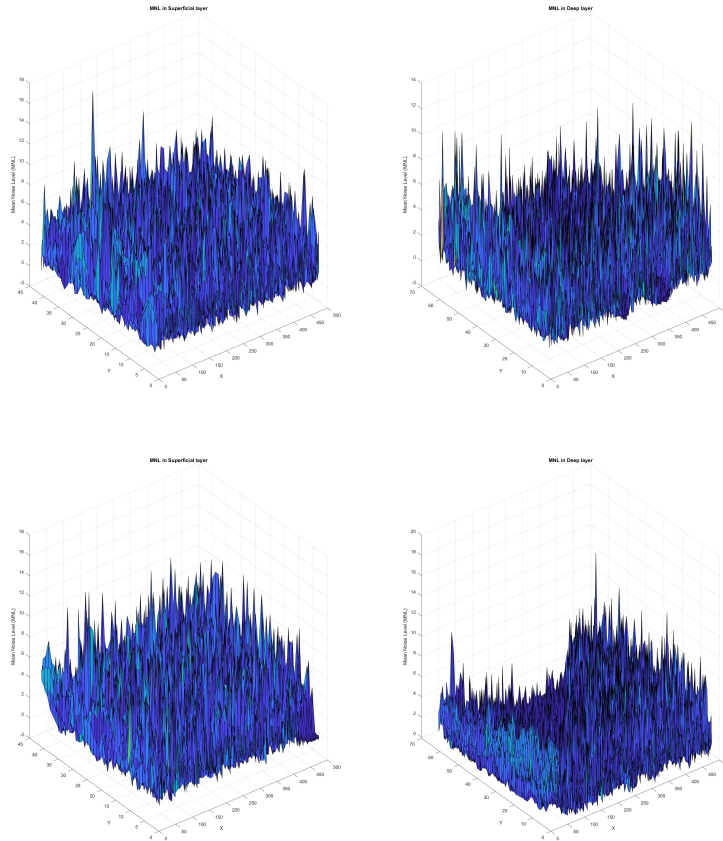


Figure 4.1: *The two graphs show the spatial distribution of Mean Noise Level (MNL): the first line belongs to an acquisition on the head at 1N, surface layer (left) and deep layer (right) respectively, the second line to the same acquisition but at 10N. One can see, qualitatively, a decrease in the value of MNL.*

representation of vascular structures.

Also, in the superficial layer, an increase in the **Skewness** value is observed as pressure increases (+5.11% for each unit increase in pressure). This could be associated with an increased presence of pixels with extreme intensity values, indicating the possible presence of artifacts or regions of outlier intensity. This effect could be related to variation in illumination, local contrast or deformation of vascular structures due to pressure exerted during acquisition.

This trend is compatible with what has been observed in other medical imaging fields, such as ultrasound, where high probe pressure can compress tissues, altering

their structure and reducing image quality. In addition, inappropriate application of pressure can change the angle of incidence of the ultrasound beam with respect to anatomical structures, adversely affecting ultrasound reflection and the resulting image quality [27], [37].

These results suggest that while moderate pressure may improve OCTA image quality by reducing noise, excessive application could have negative effects, similar to what has been observed in ultrasound. Therefore, it is critical to identify an optimal pressure range to obtain high-quality images without altering the structure of the vessels analyzed.

4.0.2 Analysis by anatomical regions

The analysis conducted for the different anatomical regions showed significant differences, related to the effect of pressure on OCTA image quality. Of all areas considered, the head showed the most significant changes in quality parameters, suggesting greater sensitivity to pressure than the arm and leg. In particular, in the head, a significant reduction in Mean Noise Level (-9.35% in the superficial layer and -6.20% in the deep layer) and PIQE (-6.60% in the superficial layer) is observed, indicating an improvement in image quality with less noise perception. At the same time, PSNR increases (about +1.70%), reinforcing the idea that pressure application contributes to a more favorable signal-to-noise ratio. However, there is also an increase in Skewness (+10.22%), suggesting a greater presence of pixels with extreme intensities, which could be due to artifacts or variations in the distribution of intensity values. In addition, there is a reduction in vascular density (-2.94%), which can be supposed as an effect of compression of blood vessels under pressure.

A distinctive aspect of the head macroarea is that, unlike arm and leg, an analysis with pressure of 1N was included. This choice was motivated by a preliminary qualitative evaluation, in which the images acquired with this pressure appeared visually better than the other conditions tested (Fig.3.13). Therefore, it was considered appropriate to include this acquisition in the study for more detailed quantitative analysis.

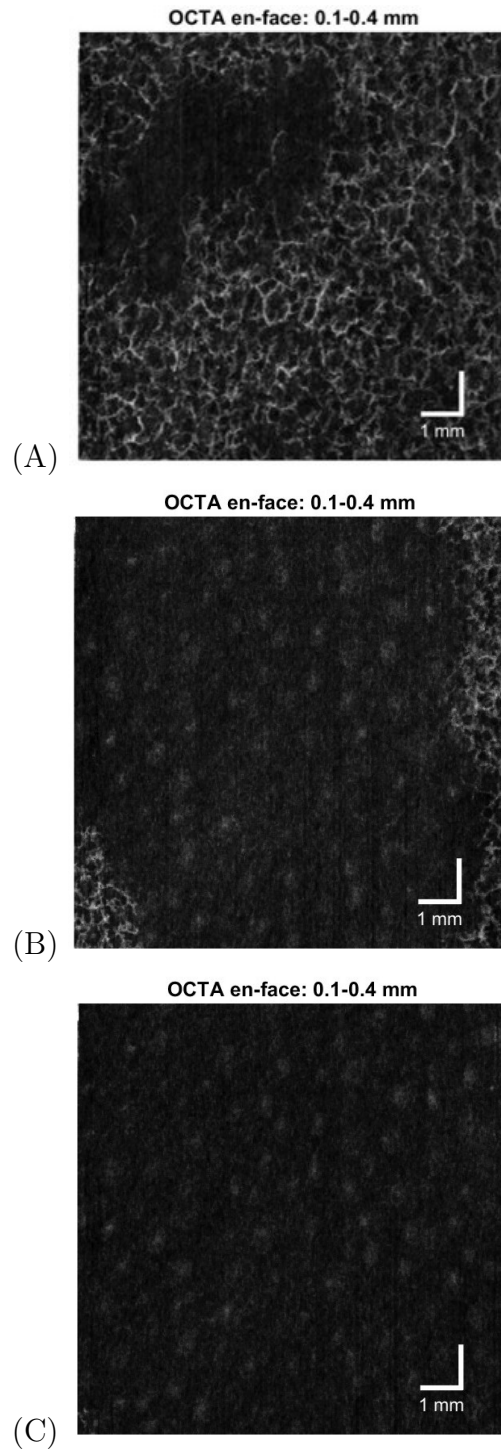


Figure 4.2: OCTA images referred to an acquisition on the head, at 1N (A), 2N (B), 4N(C). It can be seen that as the force applied by the probe increases, the vascular structure is no longer detected and is almost absent.

Another notable result concerns vascular density, a parameter for which the head is the only macroarea to show a statistically significant difference in linear regression. However, Tukey's post-hoc test results indicate that this difference is significant only between arm and leg ($p = 0.021377$), while the comparison between head and the other regions is not significant. This suggests that the variation in vascular density may not be exclusively related to applied pressure, but may depend on anatomical factors or the intrinsic vascular structure of different body regions.

In the arm, the most significant changes are in the BRISQUE parameter, with an increase in both the superficial layer (+3.84%) and the deep layer (+2.59%). This suggests that the effect of pressure in this region has less impact than in the head, affecting more the image distortion perception than a real noise reduction. The ANOVA test for BRISQUE confirmed a significant difference between the body areas, with Tukey's post-hoc test showing a difference between arm and head ($p=0.024$), but not between the other combinations.

Regarding entropy, the ANOVA test showed a highly significant difference between the macroareas ($p_{ANOVA}=1.09e-04$), with Tukey's post-hoc test showing significant differences between arm and head ($p=0.001$) and between head and leg ($p=0.0002$), while the comparison between arm and leg was not significant. This result indicates that the structural complexity of the images varies significantly between head and other macroareas, suggesting a greater influence of pressure in the cranial region.

Finally, in the leg, the only statistically significant parameter is the reduction in entropy (-1.74%): this could indicate less structural complexity in OCTA images with increasing pressure. However, unlike the head and arm, the effect of pressure in this macroarea seems to be less marked.

These results highlight how the influence of pressure on OCTA image quality is not uniform among different body regions. The head appears particularly sensitive to pressure variation, showing improvements in image quality but also the presence of possible artifacts. The arm shows smaller effects, with variations in parameters related to the perception of image quality, while in the leg the effect of pressure seems to be more limited. Moreover, the statistical significance of BRISQUE and Entropy, and to a lesser extent of Vascular Density, suggests that the effect of pressure is not only manifested in terms of noise and contrast, but also in the overall image structure. Thus, the need to calibrate pressure application according to anatomical area is evident to ensure optimal OCTA image acquisition [35], [36].

4.0.3 Pressure impact on vascular density

The analysis of vascular density was conducted through two separate methods: calculation on the binarized mask and calculation on the skeleton. Comparison of these two different techniques showed significant differences in the trend of vascular density in relation to applied pressure, with trends not always consistent between different body areas.

When vascular density is calculated on the binarized mask, a uniform decrease is observed in all acquisitions, regardless of body area and layer considered. This result suggests that increased pressure reduces the overall amount of vascular signal detected, probably due to tissue compression and subsequent reduction in surface perfusion. This effect may also result from reduced visibility of thinner vessels in OCTA images acquired with higher pressures [38].

In contrast, the calculation of vascular density on the skeleton shows a more complex and anatomical region-dependent behavior. In particular, a decrease in vascular density is observed in the head and leg, whereas in the arm the value tends to increase with pressure. This result could be explained by differences in tissue response to compression: in the head, the presence of rigid bone structures could accentuate the effect of pressure, reducing perfusion and therefore the measured vascular density. In the leg, the lower presence of superficial vascular structures could bring about a similar response, with a reduction in vascular density observed as pressure increases. By contrast, in the arm, the greater muscle component could support a compensation of blood flow following compression, with an apparent increase in vascular density when calculated on the skeleton.

These results (Fig.4.3) highlight how the calculation method significantly affects the interpretation of vascular density and how the effect of pressure is not uniform among different body areas. The decrease in vascular density in the binarized mask suggests that increasing pressure reduces the overall signal, while the variations observed in the calculation on the skeleton indicate that the response of the vascular network to pressure may vary by anatomical region and tissue type [39], [40]. These differences emphasize the importance of contextualized interpretation of the results, considering the calculation method and the specific characteristics of each body area analyzed [41], [42].

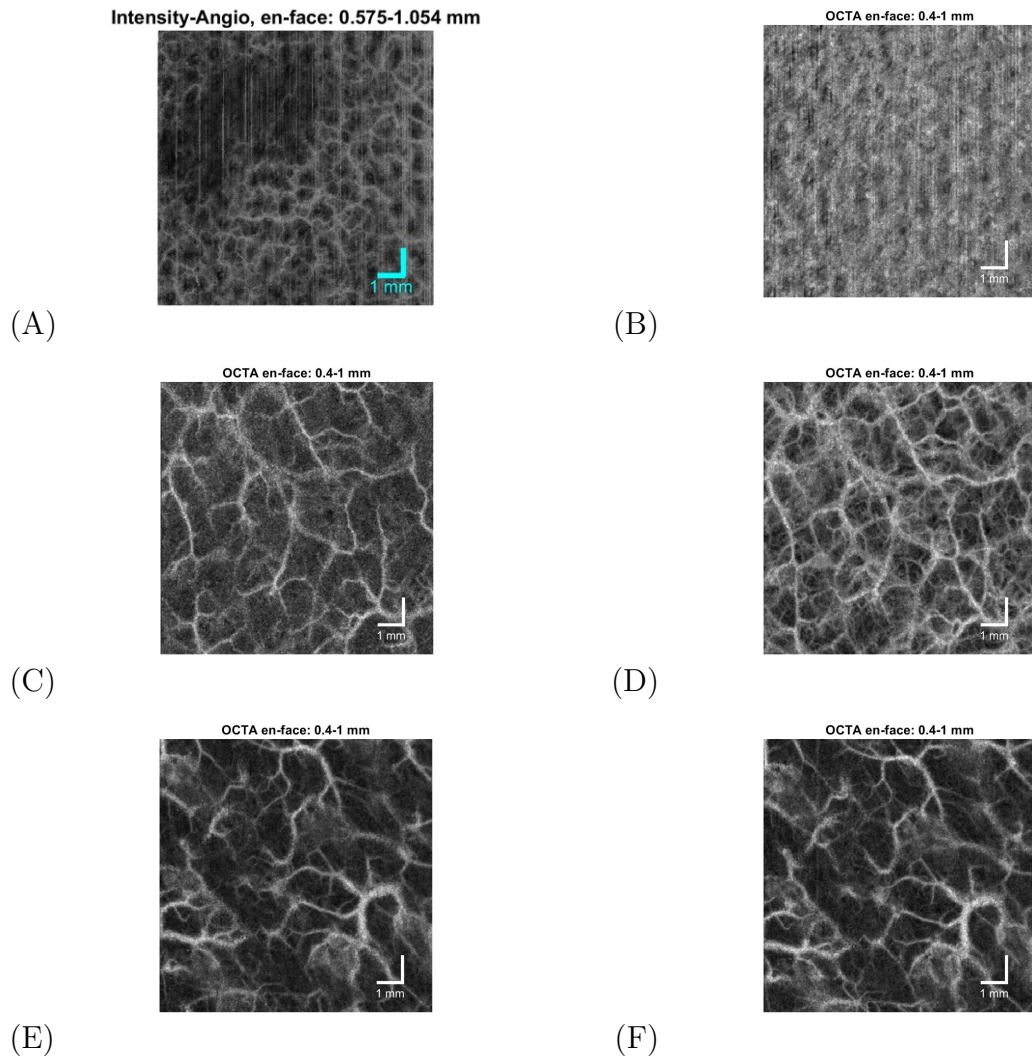


Figure 4.3: *The first row corresponds to an acquisition of the head, the second to the arm, and the third to the leg. Images in the left column (A, C,E) were taken at the minimum pressure (1N for head, 2N for arm and leg), while the images in the right column (B,D,F) were acquired at the maximum pressure (10N). In line with the results, a decrease in vascular density is observed in the head and leg acquisitions, whereas a slight increase is noticeable in the arm acquisition.*

4.0.4 Optimal pressure range

Analysis of pressure ranges applied to different body regions highlights significant differences in tissue response to compression. These data suggest that vascular density varies according to anatomical structure and the ability of tissues to balance blood flow under pressure [43], [44].

The arm is distinguished by its higher tolerance to pressure, with values between 6,91-9,47 N in both superficial and deep layers. This characteristic could be related to the presence of a significant muscular component, which promotes a more homogeneous distribution of pressure and less reduction in perfusion.

In contrast, the head shows greater sensitivity to compression, with a lower pressure range between 0,87-4 N. This behavior can be explained by the rigidity of the bony structures of the skull, which limits the ability of the tissues to adapt to pressure without compromising blood flow.

The leg is in an in between position, with pressures ranging between 1,94-8,78 N. The deep layers appear to be more resistant to compression, with values between 3,64-5,32 N, while in the superficial layers the response differs more. This response behavior could be due to the lower presence of superficial vascular structures, which makes the tissue less capable of maintaining steady flow under compression [45]. From a biomechanical perspective, this difference in behavior between deep and superficial layers can be explained by the different tissue composition. In the deep layers, the combination of greater vascular density and stronger connective tissue allows a more stable circulation to be maintained, even under high pressure. In contrast, in the superficial layers, the structure is more elastic and less vascularized: this makes the tissue more affected by compression and leads to reduced blood flow. This may explain why OCTA images of the superficial layers are more changeable as a function of applied pressure.

In summary, the data suggest that vascular density responds differently to pressure depending on body area. The head is the most sensitive to compression, followed by the leg, while the arm shows greater adaptive capacity, probably due to its muscular structure. These variations depend on tissue composition and the presence of rigid structures, which directly influence the ability of the vascular system to react to applied pressure [46], [47], [48] .

4.1 Limitations

In the interpretation of the results, it is important to consider some limitations that the study has.

A first limitation concerns the presence of artifacts during OCTA image acquisition, due to small unintentional movements of the subjects or changes in probe position. These factors may have influenced the quality of the images, compromising the reliability of the measurements, particularly in acquisitions made with higher pressures, where contact with the tissue is more unstable.

An additional limitation is the sample size, which includes only 10 acquisitions. Although the number of participants is sufficient for preliminary analysis, its small size may limit the representativeness of the results, making it difficult to generalize to a larger population.

Another aspect to consider is the limited choice of anatomical regions analyzed, which focused exclusively on three areas of the body: arm, forehead and leg. Although these areas were selected to represent tissues with different structural characteristics, their analysis does not allow for a full exploration of the variability of vascular response to pressure in other parts of the body, which might perform differently depending on their tissue structure and vascular density.

Finally, it is important to point out some technical limitations related to the OCTA acquisition system. The spatial resolution of the instrument, although high, may not be sufficient to detect thinner capillaries accurately, especially under higher pressure conditions, where tissue compression could further reduce the visibility of smaller vessels. In addition, OCTA's penetration depth is limited, making it difficult to analyze deeper tissue layers that might respond differently to pressure.

Chapter 5

Conclusions and Future Developments

This study analyzed the effect of probe pressure on the quality of skin OCTA images, highlighting significant differences among the body regions examined and among the computational methods used. In general, it can be stated that increased pressure has a more pronounced impact on superficial layers than on deep layers, suggesting that tissue compression has a determining effect on the reduction of the detected vascular signal.

A relevant aspect that emerged concerns noise-related parameters, such as Mean Noise Level and PSNR, which showed significant variations. These results indicate that applying a given pressure can, in some cases, improve the quality of OCTA images by reducing background noise and improving the contrast of thinner blood vessels.

Anatomically, the head region is distinguished by significant variations in multiple parameters, related to noise, image quality and texture, suggesting greater sensitivity to pressure than the arm and leg. This could be attributed to the presence of rigid bony structures near the area of probe application, and less vascular adaptability than the muscle tissues of the arm and leg.

In addition, the study showed that vascular density varies according to the region analyzed and the calculation method employed. The use of the binarized mask results in a uniform decrease in vascular density in all areas with increasing pressure, while the skeleton method shows more complex and anatomical structure-dependent responses. Among the regions analyzed, the leg showed the most marked reduction in vascular density, suggesting that less superficially vascularized tissues are more

susceptible to compression.

Finally, analysis of optimal pressure ranges showed differences between body areas and tissue layers, highlighting the need to accurately calibrate applied pressure to obtain optimal images in different body regions. This is particularly relevant for OCTA-based clinical and diagnostic studies, where the pressure applied could affect image quality and interpretation.

The results obtained suggest several possible future developments. A first step would be to expand the study sample to include a larger number of subjects to improve the statistical significance of the data and test its reproducibility in a larger population. In addition, it would be valuable to extend the analysis to other anatomical regions to evaluate whether the vascular response to pressure follows similar trends or whether there are further tissue structure-dependent differences. Further improvement could involve optimizing the acquisition methodology, through the use of devices to stabilize the OCTA probe, reducing the risk of artifacts due to subjects' involuntary movements.

These developments would enable improved analysis methodologies, improving the quality of OCTA images and potentially expanding their applicability in clinical and diagnostic settings.

Bibliography

- [1] «Anatomy, histology and immunohistochemistry of normal human skin». In: *European Journal of Dermatology* (). John Libbey Eurotext (cit. on p. 2).
- [2] R. Wong, S. Geyer, W. Weninger, J. Guimberteau, and J. K. Wong. «The dynamic anatomy and patterning of skin». In: *Experimental Dermatology* 25.2 (Feb. 2016), pp. 92–98. DOI: 10.1111/exd.12832 (cit. on p. 2).
- [3] Z. Lotfollahi. «The anatomy, physiology and function of all skin layers and the impact of ageing on the skin». In: *Wound Practice and Research* 32.1 (Mar. 2024). DOI: 10.33235/wpr.32.1.6–10 (cit. on p. 2).
- [4] Minjun Ahn, Won-Woo Cho, Park Wonbin, Jae-Seong Lee, Min-Ju Choi, Qiqi Gao, Ge Gao, and Byoung Kim. «3D biofabrication of diseased human skin models in vitro». In: *Biomaterials Research* 27 (Aug. 2023). DOI: 10.1186/s40824-023-00415-5 (cit. on p. 3).
- [5] H.-C. Park et al. «Minimizing OCT quantification error via a surface-tracking imaging probe». In: *Biomedical Optics Express* 12.7 (July 2021), p. 3992. DOI: 10.1364/B0E.423233 (cit. on p. 4).
- [6] L. Veselka, L. Krainz, L. Mindrinos, W. Drexler, and P. Elbau. «A Quantitative Model for Optical Coherence Tomography». In: *Sensors* 21.20 (Oct. 2021), p. 6864. DOI: 10.3390/s21206864 (cit. on p. 4).
- [7] W. Brown, K. Chu, and D. S. Whitney. «Optical Coherence Tomography». In: () (cit. on p. 4).
- [8] Encyclopædia Britannica. *Light*. Accessed: March 6, 2025. n.d. URL: <https://www.britannica.com/science/light> (cit. on p. 5).
- [9] Pionline. *Tomografia a Coerenza Ottica (OCT)*. Accessed: March 6, 2025. n.d. URL: <https://www.pionline.it/it/esperienza/mercati/microscopia-life-sciences/endoscopia-diagnostica-in-vivo/tomografia-a-coerenza-ottica-oct> (cit. on p. 6).
- [10] R. Leitgeb, C. Hitzenberger, and A. Fercher. «Performance of fourier domain vs time domain optical coherence tomography». In: *Opt. Express* 11.8 (Apr. 2003), p. 889. DOI: 10.1364/OE.11.000889 (cit. on p. 7).

-
- [11] et al. M. Zeppieri. «Optical Coherence Tomography (OCT): A Brief Look at the Uses and Technological Evolution of Ophthalmology». In: *Medicina (Mex.)* 59.12 (Dec. 2023), p. 2114. DOI: 10.3390/medicina59122114 (cit. on p. 7).
- [12] Enaholo ES, Musa MJ, and Zeppieri M. *Optical Coherence Tomography*. In: StatPearls [Internet]. Treasure Island (FL): StatPearls Publishing; 2025 Jan-. Available from: <https://www.ncbi.nlm.nih.gov/books/NBK606122/>. Updated October 6. 2024 (cit. on p. 7).
- [13] D. P. Popescu and et al. «Optical coherence tomography: fundamental principles, instrumental designs and biomedical applications». In: *Biophys. Rev.* 3.3 (Sept. 2011), pp. 155–169. DOI: 10.1007/s12551-011-0054-7 (cit. on p. 7).
- [14] et al. Z. Chen. «Phase-stable swept source OCT angiography in human skin using an akinetic source». In: *Biomed. Opt. Express* 7.8 (Aug. 2016), p. 3032. DOI: 10.1364/B0E.7.003032 (cit. on p. 7).
- [15] S. Aumann, S. Donner, J. Fischer, and F. Müller. «Optical Coherence Tomography (OCT): Principle and Technical Realization». In: *High Resolution Imaging in Microscopy and Ophthalmology*. Ed. by J. F. Bille. Cham: Springer International Publishing, 2019, pp. 59–85. DOI: 10.1007/978-3-030-16638-0_3 (cit. on p. 8).
- [16] De Carlo TE, Romano A, Waheed NK, and Duker JS. *A review of optical coherence tomography angiography (OCTA)*. Dec. 2015. DOI: 10.1186/s40942-015-0005-8 (cit. on p. 7).
- [17] Tan ACS et al. *An overview of the clinical applications of optical coherence tomography angiography*. Feb. 2018. DOI: 10.1038/eye.2017.181 (cit. on p. 9).
- [18] Wylegała A. *Principles of OCTA and Applications in Clinical Neurology*. Dec. 2018. DOI: 10.1007/s11910-018-0911-x (cit. on p. 9).
- [19] Spaide RF, Fujimoto JG, Waheed NK, Sadda SR, and Staurenghi G. *Optical coherence tomography angiography*. May 2018. DOI: 10.1016/j.preteyeres.2017.11.003 (cit. on p. 10).
- [20] Le PH, Kaur K, and Patel BC. *Optical Coherence Tomography Angiography*. In: StatPearls [Internet]. Treasure Island (FL): StatPearls Publishing; 2025 Jan-. Available from: <https://www.ncbi.nlm.nih.gov/books/NBK563235/>. Updated October 6. 2024 (cit. on p. 10).
- [21] Naseripour M, Ghasemi Falavarjani K, Mirshahi R, and Sedaghat A. *Optical coherence tomography angiography (OCTA) applications in ocular oncology*. Sept. 2020. DOI: 10.1038/s41433-020-0819-y (cit. on p. 10).

- [22] ME-Meßsysteme GmbH. *KD34s 10N Force Sensor Datasheet*. Technical specifications of the KD34s 10N force sensor. ME-Meßsysteme GmbH. Eduard-Maurer-Str. 9, DE-16761 Hennigsdorf, 2025. URL: <https://www.me-systeme.de> (cit. on p. 10).
- [23] F. D. Fuchs and P. K. Whelton. «High Blood Pressure and Cardiovascular Disease». In: *Hypertension* 75.2 (Feb. 2020), pp. 285–292. DOI: 10.1161/HYPERTENSIONAHA.119.14240 (cit. on p. 12).
- [24] J. D. Pleil, M. Ariel Geer Wallace, M. D. Davis, and C. M. Matty. «The physics of human breathing: flow, timing, volume, and pressure parameters for normal, on-demand, and ventilator respiration». In: *Journal of Breath Research* 15.4 (Oct. 2021). DOI: 10.1088/1752-7163/ac2589 (cit. on p. 13).
- [25] R. Machiele, M. Motlagh, and M. Zeppieri. «Intraocular Pressure». In: *StatPearls [Internet]* (). Updated 2024 Feb 27, StatPearls Publishing; 2025 Jan (cit. on p. 14).
- [26] V. M. Runge. «Safety of approved MR contrast media for intravenous injection». In: *Journal of Magnetic Resonance Imaging* 12.2 (Aug. 2000), pp. 205–213. DOI: 10.1002/1522-2586(200008)12:2<205::AID-JMRI1>3.0.CO;2-P (cit. on p. 14).
- [27] S. Ødegaard, M. B. Kimmey, R. W. Martin, H. C. Yee, A. H. S. Cheung, and F. E. Silverstein. «The effects of applied pressure on the thickness, layers, and echogenicity of gastrointestinal wall ultrasound images». In: *Gastrointestinal Endoscopy* 38.3 (May 1992), pp. 351–356. DOI: 10.1016/S0016-5107(92)70431-3 (cit. on pp. 15, 59).
- [28] Q. Li, F. Zhang, Q. Xi, Z. Jiao, and X. Ni. «Nondeformed Ultrasound Image Production Method for Ultrasound-Guided Radiotherapy». In: *Technology in Cancer Research Treatment* 22 (Jan. 2023). DOI: 10.1177/15330338231194546 (cit. on p. 15).
- [29] M. Hamza, R. Skidanov, and V. Podlipnov. «Visualization of Subcutaneous Blood Vessels Based on Hyperspectral Imaging and Three-Wavelength Index Images». In: *Sensors* 23.21 (Nov. 2023), p. 8895. DOI: 10.3390/s23218895 (cit. on p. 15).
- [30] A. J. Deegan et al. «Optical coherence tomography angiography of normal skin and inflammatory dermatologic conditions». In: *Lasers in Surgery and Medicine* 50.3 (Mar. 2018), pp. 183–193. DOI: 10.1002/lsm.22788 (cit. on p. 15).
- [31] K. M. Meiburger et al. «Automatic skin lesion area determination of basal cell carcinoma using optical coherence tomography angiography and a skeletonization approach: Preliminary results». In: *Journal of Biophotonics* 12.9 (Sept. 2019). DOI: 10.1002/jbio.201900131 (cit. on p. 15).

- [32] Y. Shi, J. Lu, N. Le, and R. K. Wang. «Integrating a pressure sensor with an OCT handheld probe to facilitate imaging of microvascular information in skin tissue beds». In: *Biomedical Optics Express* 13.11 (Nov. 2022), p. 6153. DOI: 10.1364/B0E.473013 (cit. on p. 15).
- [33] M. Wang-Evers et al. «Assessing the impact of aging and blood pressure on dermal microvasculature by reactive hyperemia optical coherence tomography angiography». In: *Scientific Reports* 11.1 (June 2021), p. 13411. DOI: 10.1038/s41598-021-92712-z (cit. on p. 16).
- [34] R. F. Spaide, J. G. Fujimoto, and N. K. Waheed. «IMAGE ARTIFACTS IN OPTICAL COHERENCE TOMOGRAPHY ANGIOGRAPHY». In: *Retina* 35.11 (Nov. 2015), pp. 2163–2180. DOI: 10.1097/IAE.0000000000000765 (cit. on p. 28).
- [35] J. Gu, J. Liao, T. Zhang, Y. Zhang, Z. Huang, and C. Li. «Quantitative Optimization of Handheld Probe External Pressure on Dermatological Microvasculature Using Optical Coherence Tomography-Based Angiography». In: *Micromachines* 15.9 (Sept. 2024), p. 1128. DOI: 10.3390/mi15091128 (cit. on pp. 32, 61).
- [36] Y. Su, X. S. Yao, C. Wei, Y. Wang, H. Wang, and Z. Li. «Determination of the Pressure Coefficient of Optical Attenuation in Different Layers of In-Vivo Human». In: *Journal Name* XX.X (Month 2024), pp. XXX–XXX. DOI: DOI (cit. on pp. 32, 61).
- [37] Q. Li, F. Zhang, Q. Xi, Z. Jiao, and X. Ni. «Nondeformed Ultrasound Image Production Method for Ultrasound-Guided Radiotherapy». In: *Technology in Cancer Research Treatment* 22 (Jan. 2023), p. 15330338231194546. DOI: 10.1177/15330338231194546 (cit. on p. 59).
- [38] M. Casper, H. Schulz-Hildebrandt, M. Evers, R. Birngruber, D. Manstein, and G. Hüttmann. «Optimization-based vessel segmentation pipeline for robust quantification of capillary networks in skin with optical coherence tomography angiography». In: *Journal of Biomedical Optics* 24.4 (Apr. 2019), p. 1. DOI: 10.1117/1.JBO.24.4.046005 (cit. on p. 62).
- [39] F. Abdolahi et al. «Optical Coherence Tomography Angiography-Derived Flux As a Measure of Physiological Changes in Retinal Capillary Blood Flow». In: *Translational Vision Science Technology* 10.9 (Aug. 2021), p. 5. DOI: 10.1167/tvst.10.9.5 (cit. on p. 62).
- [40] W. Xue et al. «In vivo Noninvasive Imaging and Quantitative Analysis of Iris Vessels». In: *Ophthalmic Research* 64.5 (2021), pp. 754–761. DOI: 10.1159/000516553 (cit. on p. 62).

- [41] H. B. Lim, Y. W. Kim, J. M. Kim, Y. J. Jo, and J. Y. Kim. «The Importance of Signal Strength in Quantitative Assessment of Retinal Vessel Density Using Optical Coherence Tomography Angiography». In: *Scientific Reports* 8.1 (Aug. 2018), p. 12897. DOI: 10.1038/s41598-018-31321-9 (cit. on p. 62).
- [42] A. Y. Kim, Z. Chu, A. Shahidzadeh, R. K. Wang, C. A. Puliafito, and A. H. Kashani. «Quantifying Microvascular Density and Morphology in Diabetic Retinopathy Using Spectral-Domain Optical Coherence Tomography Angiography». In: *Investigative Ophthalmology Visual Science* 57.9 (July 2016), OCT362. DOI: 10.1167/iovs.15-18904 (cit. on p. 62).
- [43] A. Himawan. «Development of Hydrogel-Forming Microneedle Array Patches for Transdermal Protein Biomarker Sampling». PhD thesis. 2023 (cit. on p. 64).
- [44] M. A. Kirby et al. «Probing elastic anisotropy of human skin in vivo with light using non-contact acoustic micro-tapping OCE and polarization sensitive OCT». In: *Scientific Reports* 12.1 (Mar. 2022), p. 3963. DOI: 10.1038/s41598-022-07775-3 (cit. on p. 64).
- [45] W. J. Choi, Y. Li, and R. K. Wang. «Monitoring Acute Stroke Progression: Multi-Parametric OCT Imaging of Cortical Perfusion, Flow, and Tissue Scattering in a Mouse Model of Permanent Focal Ischemia». In: *IEEE Transactions on Medical Imaging* 38.6 (June 2019), pp. 1427–1437. DOI: 10.1109/TMI.2019.2895779 (cit. on p. 64).
- [46] Z. Xie, G. Wang, Y. Cheng, Q. Zhang, M. N. Le, and R. K. Wang. «Optical coherence tomography angiography measures blood pulsatile waveforms at variable tissue depths». In: *Quantitative Imaging in Medicine and Surgery* 11.3 (Mar. 2020), pp. 907–917. DOI: 10.21037/qims-20-778 (cit. on p. 64).
- [47] A. K. Durrani. *Advancing optical coherence tomography angiography towards the better diagnosis of cutaneous microvascular disease*. 2023 (cit. on p. 64).
- [48] K. Lewandowska et al. «Methods for the assessment of microcirculation in patients with hypertension». In: *Arterial Hypertension* 27.1 (Mar. 2023), pp. 1–12. DOI: 10.5603/AH.a2023.0004 (cit. on p. 64).